Accepted for Publication in the Astronomical Journal, July 2002

The Dwarf Spheroidal Companions to M31: WFPC2 Observations of Andromeda III[1]

G. S. Da Costa

Research School of Astronomy & Astrophysics, Institute of Advanced Studies, The Australian National University, Cotter Road, Weston, ACT 2611, Australia

gdc@mso.anu.edu.au

T. E. Armandroff

National Optical Astronomy Observatory, P.O. Box 26732, Tucson, Arizona 85726

armand@noao.edu

and

Nelson Caldwell

Smithsonian Astrophysical Observatory, 60 Garden Street, Cambridge, MA 02138

caldwell@cfa.harvard.edu

ABSTRACT

The *Hubble Space Telescope* WFPC2 camera has been used to image Andromeda III, a dwarf spheroidal (dSph) companion to M31. The resulting color-magnitude (c-m) diagrams reveal for the first time the morphology of the horizontal branch (HB) in this dwarf galaxy. We find that like Andromeda I and Andromeda II, and like most of the Galactic dSph companions, the HB morphology of And III is predominantly red, redder indeed than that of both And I and And II despite And III having a lower mean metallicity. The And III HB morphology is also somewhat redder than that of the Galactic dSph Draco, which has a similar mean abundance to And III. We interpret this red HB morphology as indicating that the bulk of the And III population is $\sim$3 Gyr younger than the age of the majority of Galactic globular clusters. Nevertheless, the And III c-m diagram does reveal the presence of a few blue HB stars, and a number of RR Lyrae variables are also evident in the data. This indicates that And III does contain an "old" population of age comparable to that of the Galactic globular clusters. There is no evidence, however, for any young stars in And III despite a claimed association between this dSph and an HI cloud. As was the case for And II, but not And I, no

radial gradient was detected in the And III horizontal branch morphology. The mean V magnitude of the horizontal branch is 25.06 ± 0.04 leading to $(m - M)_0 = 24.38 \pm 0.06$ for this dwarf. And III is then ∼75 kpc from the center of M31, comparable to the Galactocentric distances of Sculptor and Draco. Comparison with standard globular cluster red giant branches indicates a mean abundance for And III of <[Fe/H]> = –1.88 ± 0.11, the lowest mean abundance of any of M31's companions. This value, however, is consistent with the absolute magnitude – mean abundance relation followed by dSph galaxies. The same comparison yields an intrinsic abundance dispersion for And III of $\sigma_{int}([Fe/H]) = 0.12$, a low value compared to And I and And II and to the Galactic dSphs of comparable luminosity to And III. If confirmed by future spectroscopic studies, this low value would suggest that And III retained relatively little of the enrichment products generated during its evolutionary history. The list of candidate variables reveals one definite and one probable Anomalous Cepheid variable stars in And III. Such variables are common in Galactic dSphs, so their discovery in And III is not unexpected.

Subject headings: galaxies: dwarf — galaxies: individual (Andromeda III) — galaxies: photometry — galaxies: stellar content — galaxies: abundances — Local Group

1. Introduction

The Galaxy's dwarf spheroidal (dSph) companions show a surprising diversity in the epochs of their *major* star formation episode(s): for some galaxies that epoch occurred ∼15 Gyr ago while for others it was as recent as ∼2–3 Gyr ago. In addition, the majority of the Galaxy's nine dSph companions have had extended star formation histories. These histories are also diverse, with multiple distinct episodes of star formation in some systems and approximately continuous star formation over a significant fraction of the Hubble time in others (see, for example, Da Costa (1998), Grebel (1999) and Mateo (1998)).

This variety of star formation histories was initially hinted at by the range of horizontal branch (HB) morphologies seen in the Galactic dSphs. For the majority of Galactic globular clusters, there is a well established relation between metal abundance and HB morphology. This relation arises from the fact that the globular clusters of the Galaxy, especially those in the inner halo, are essentially coeval (e.g. Lee et al. (1994)). Consequently, if the mean abundance of a stellar system is known, then it is possible to predict the HB morphology expected if the dominant stellar population has an age comparable to the majority of Galactic globular clusters. When this test is

[1]Based on observations with the NASA/ESA *Hubble Space Telescope*, obtained at the Space Telescope Science Institute, which is operated by the Association of Universities for Research in Astronomy, Inc., (AURA), under NASA Contract NAS 5-26555.

applied to the dSph companions of the Galaxy, however, most have redder HBs than predicted. In other words a "second parameter" is needed to explain their HB morphologies.

The prime candidate for the "second parameter" is age, since younger, higher mass stars are cooler (redder) in their core helium burning phase of evolution. For the Galactic globular clusters, the interpretation of the second parameter as age remains controversial, though there are pairs of globular clusters of similar abundance but different HB morphologies where an age difference is well established, such as NGC 288 and 362 (Green & Norris (1990), Bellazzini et al. (2001); see also Stetson et al. (1999), Rey et al. (2001) and the references therein). But for dSphs, there is little reason to question the assertion that metal-poor systems with strong red HBs have mean ages younger than the Galactic globular clusters. Indeed, the assertion is given credence by direct determinations of the mean ages of Galactic dSphs, via measurement of the main sequence turnoff luminosity. For example, main sequence photometry of Carina (Smecker-Hane et al. 1996; Hurley-Keller et al. 1998) clearly shows the turnoff of an old population ($\sim$15 Gyr), which provides the progenitors for the RR Lyrae and blue HB stars observed in this dSph. Also visible is the turnoff of the dominant intermediate-age ($\sim$4–6 Gyr) population, which produces the numerous "red clump" stars – intermediate-age stars in the core helium burning phase of evolution. Other examples where direct measurement of the main sequence turnoff connects a mean age younger than that of the Galactic globular clusters with a red HB morphology include Leo II (Mighell & Rich 1996), Leo I (Gallart et al. 1999), and Fornax (Stetson et al. 1998). Ursa Minor, which has the blue HB expected for its low metallicity and the assumption of a dominant old population, also fits this picture; main sequence turnoff observations confirm that this dSph is indistinguishable in age from the Galactic globular clusters (Olszewski & Aaronson 1985; Mighell & Burke 1999).

While these recent observations have revealed the diversity of star formation histories among the Galactic dSphs, there is no accepted explanation for its origin, only hints. For example, there is a tendency for Galactic dSphs with younger mean ages to lie at larger distances from the Galaxy (van den Bergh 1994). Clearly, we need to study additional dSphs if we are to understand the origin of this diversity. The nearest dSph galaxies beyond the Galaxy's companions are the dSph companions to M31. The availability of WFPC2 on the *Hubble Space Telescope* allows accurate photometry at magnitudes fainter than the horizontal branch in M31's dSph companions. We have used *HST*/WFPC2 to obtain photometry for stars in two of M31's dSph companions, And I and And II (Da Costa et al. 1996, 2000). The resulting color-magnitude diagrams for these dSphs reveal strong red HB morphologies. These morphologies are considerably redder than that expected from the mean abundances of the dSphs, when coupled with the assumption of a dominant stellar population similar in age to the Galactic globular clusters. Instead, the HB morphologies indicate that the bulk of the population in And I and II is younger than the Galactic globular clusters. In addition, the And I and II color-magnitude diagrams have been used to derive accurate distances, from the mean magnitude of the horizontal branch, and to determine each galaxy's abundance distribution, from the colors of the red giants (Da Costa et al. (1996, 2000); hereafter Paper I and Paper II, respectively).

In this paper, we use similar *HST*/WFPC2 data and analysis techniques to those of Papers I and II to study Andromeda III. And III is one of the least luminous ($M_V \approx$ –10.2, Caldwell et al. (1992)), and is apparently the most metal-poor ([Fe/H] $\approx$ –2.0, Armandroff et al. (1993)), of the M31 dSph (and dE) companions. It lies between And I and And II in projected distance from the center of M31. Armandroff et al. (1993), hereafter ADCS93, have presented a ground-based color-magnitude diagram for And III, which shows the dSph's upper giant branch. These authors suggest that the fraction of intermediate-age (age between ∼3 and 10 Gyr) population in this dSph is approximately 10 ± 10 percent. And III is of additional interest because of the claim of Blitz & Robishaw (2000) that this dSph is associated with a H I cloud. In most, but not all situations (cf. Sculptor, Carignan et al. (1998)), association with a H I cloud is reflected in the stellar population of the dSph, via the presence of young stars (e.g. Phoenix, Holtzman et al. (2000); LGS 3, Aparicio et al. (1997); Miller et al. (2001)).

The remainder of this paper is split into three sections. In §2 the observations, photometry techniques and calibration processes are described. Section 3 presents the main results of the paper. These include, inter alia, the HB morphology, the distance of And III from the center of M31, the mean abundance and abundance dispersion, and implications for the age of the bulk of And III's stellar population. The final section discusses the results in the wider context of dSph evolution.

2. Observations and Reductions

Andromeda III was imaged with the WFPC2 instrument aboard the *Hubble Space Telescope* on 1999 February 22 and again, at the same orientation, on 1999 February 26 as per our GO program 7500. Both sets of observations consisted of four 1200 s integrations through the F555W ("Wide-V") filter and eight 1300 s integrations through the F450W ("Wide-B") filter. And III is a highly flattened system ($b/a \approx 0.4$, Caldwell et al. (1992)) and so an orientation range was specified at the proposal Phase-II stage to ensure the major axis of the galaxy lay approximately across the WF2 and WF4 chips. Further, the WFALL-FIX center employed was offset somewhat from the actual center of the dSph in order to ensure that all bright foreground stars (cf. ADCS93, Fig. 2) fell well outside the WFPC2 field-of-view for the orientation range specified. The actual observations placed the center of And III on the WF2 chip, approximately 18″ from the WFPC2 pyramid apex. The orientation of the observations differed only by about 4 degrees from that required to place the And III major axis along the WF2–WF4 diagonal (U2, V2 axes). This difference is within the uncertainty of the determination of the And III major-axis position angle. As for our previous observations of And I and And II, the second set of And III observations was offset from the first by a small amount, nominally 9.5 WF pixels in both x and y. This facilitates distinguishing real stars from instrumental defects, such as hot pixels, and allows an assessment of the errors in the photometry.

The raw frames were processed via standard STScI pipeline procedures. The processed frames were then separated into the images for each individual CCD, multiplied by the appropriate ge-

ometric distortion image as supplied by STScI, and trimmed of the vignetted regions using the boundaries recommended in the WFPC2 Handbook. The locations of bright stars were then measured on each set (one for each combination of filter, position and CCD) to ascertain whether there were any systematic changes in position during the sequence of observations. None were found. The individual images for each set were then combined using the *gcombine* task within the STSDAS package. As for our previous WFPC2 data sets, a value of 0.10 was adopted for the *gcombine* parameter *snoise* as the best compromise between cosmic-ray rejection and ensuring that the magnitudes of bright stars on the combined frame are not significantly different ($\lesssim$0.02 mag) from the average of the values from the individual frames. Further, for these data, it was apparent that the background sky level is significantly lower on the second of the two exposures per orbit. Thus, in using *gcombine*, additive offsets were applied to bring the set of frames to the same background level before initiating the rejection process.

A mosaic made from the combination of four 1200 s F555W frames is shown in Fig. 1. As for the And I and II data, the HST/WFPC2 combination completely resolves this dSph; indeed the And III stars are relatively uncrowded. There is also no indication of any star clusters on this image (nor are there any candidates from ground-based imaging), a result that is not surprising given the relatively low luminosity of this dSph. The strong flattening of And III is also evident in this image – it is the reason for the comparative absence of stars, for example, in the parts of the WF3 chip furthest from the camera apex.

2.1. Photometry

As for And I and And II, the relatively uncrowded nature of the And III frames means that we can employ the techniques of aperture photometry. We note first, however, that as in Paper II we have not used any data from the PC1 frames. This is because the small area relative to the WF CCDs, together with its location on And III's minor axis, results in only a small addition to the total number of stars from the PC data. Further, there is also a comparative lack of "bright" stars on the PC frames with which to determine aperture corrections. Consequently, all subsequent discussion applies only to the three WF CCDs, though nevertheless, we will include the PC in our subsequent full analysis of the And III variable star content (cf. Pritzl et al. (2002)).

The photometry procedures adopted were identical to those described in Paper II. The initial image-center coordinate lists were generated with the *daofind* routine within IRAF/DAOPHOT. Aperture photometry was then carried out using a 2 pixel radius aperture with the "sky" taken as the mode of the pixel values in an annulus of inner radius 5 and outer radius 15 pixels. Typically a dozen or so of the brightest, most isolated stars distributed across each WF CCD were then used to determine the aperture corrections – the difference between the 2 pixel measurement aperture and the 5 pixel standard aperture adopted by Holtzman et al. (1995), hereafter H95. The values for the individual stars were then averaged to form a single correction for each filter/position/WF CCD combination. These values are typically uncertain by 0.01 – 0.02 mag. The corrected photometry

lists for the two positions and a given filter were then compared. There were no indications of any systematic differences and so a single magnitude was generated by averaging the two measurements. Stars detected on only one frame were discarded. Similarly, the combined photometry lists for the F555W and F450W filters were matched to produce F450W–F555W colors. Again stars not detected in both filters were ignored. At this stage corrections for exposure time, gain factors and zero-point were also applied to place the photometry on the H95 system.

As for Paper II, to minimize the effects of crowding, any star whose center lay within 5 pixels of the center of another star was removed from the photometry lists. Given the relatively uncrowded nature of these data, the number of stars removed by this process was small (typically 5%) but it did reduce the scatter in the c-m diagrams. Finally, the remaining "stars" were visually inspected on the four-exposure-combined F555W images and a few objects, mostly marginally resolved galaxies, removed. The final And III sample then consists of 1630 stars from the three WF frames.

2.1.1. Charge-Transfer Efficiency Corrections

The WFPC2 CCDs are known to suffer from poor charge-transfer efficiency (CTE) and this effect is gradually worsening with time (e.g. Whitmore et al. (1999) and references therein). Without correction, poor CTE results in systematically fainter magnitudes for stars that undergo the largest number of charge transfers (i.e. those with large x and y pixel coordinates). As was the case for Papers I and II, we have therefore chosen to correct our photometry for CTE effects. Specifically, noting that the analysis carried out by Whitmore et al. (1999) contains data obtained as recently as $\sim$2 weeks prior to our And III observations, we have used equations 1a, 1b and 3 of Whitmore et al. (1999) to correct the raw photometry for CTE effects. We then regenerated the final averaged, crowding corrected, edited and calibrated photometry list by repeating the steps outlined in the previous section. For our observations, the Whitmore et al. (1999) correction process makes a typical And III red horizontal branch star near the center of a WF frame brighter by about 0.08 mag and bluer by about 0.02 mag relative to the uncorrected photometry. The corrections are about twice as large for horizontal branch stars with large x and y coordinates. Application of the Dolphin (2000) CTE correction equations gives similar results.

2.1.2. Photometric Errors

The CTE corrected data can now be used to quantify the photometric errors as a function of magnitude. These photometric errors are those that result from the measurement process and are distinct from any systematic uncertainty in the data. The latter uncertainty arises, for example, from errors in the zero-point calibration and in the CTE correction process. To calculate the photometric errors we compared the photometry for the two separate pointings using only the stars in the final sample. The results of this process are given in Table 1 which lists, for the specified

magnitude bins, the average error for the mean of the two measures (magnitude and color). As was found in Papers I and II, for these uncrowded stars the photometric errors, particularly at fainter magnitudes, are essentially those expected on the basis of photon statistics. At the brightest levels, however, the errors asymptote to a limit of ∼0.015 mag, again as was seen in the previous analyses. This limit presumably represents the fundamental limit on the photometric precision for these data, given the effects of flat-fielding, dark subtraction and the frame combination process adopted. This limit does not affect the interpretation of the data in any way. The values in Table 1 are in fact about 20% larger than the equivalent values for the And II photometry of Paper II, despite similar exposure times. This difference has its origin in the fact that the background sky values for the And III frames are a factor of approximately two higher.

In the process of comparing the photometry for the two pointings, a small number of stars were identified as having magnitude or color differences larger by 3.5σ or more than the mean difference for their magnitude (which was always close to zero). Based on the experience of Papers I and II, it is likely that the majority of these stars with discrepant photometry are in fact variable stars, principally RR Lyraes. These stars will be discussed further in § 3.1.2. Figure 2 shows the CTE corrected color-magnitude diagram for the final And III sample on the photometric system of H95. The 22 candidate variable stars are plotted with a different symbol.

2.1.3. V and $B-V$ Zero-Points

In Paper II we used a set of ground-based deep B and V images of And II to investigate the zero-points of the transformations from F555W to V and F450W to B given by H95. It was found that the ground-based V photometry agreed well with the WFPC2 F555W photometry when transformed to V as prescribed in H95. For the B magnitudes, however, the ground-based data indicated a zero-point shift of 0.055 mag relative to the H95 F450W to B transformation, in the sense of fainter B magnitudes. This offset (and the lack of an offset in V) was confirmed by analyzing F450W and F555W observations, obtained from the HST archive, of the ω Cen standard field (Paper II). The lack of an offset in V and the presence of one in B is not too surprising given that the H95 F555W to V transformation is empirical while that for F450W to B is not (see Paper II).

For And III, however, we do not have high quality well-calibrated deep B and V images with which to perform a similar zero-point investigation. Nevertheless, as a check on our photometric zero-point in V, we have compared our WFPC2 photometry with that obtained by ADCS93 who used the KPNO 4-m telescope prime-focus CCD camera. To carry out this comparison, the WFPC2 and KPNO 4-m images were inspected and a number of stars which could be reliably measured on the ground-based images selected. These stars, which are distributed over the WF frames, are all at or near the top of the And III red giant branch. For the 19 stars in the comparison, the mean value of $V_{WFPC2} - V_{ADCS93}$ is –0.011 mag with a standard error in this mean of 0.013 mag. Excluding the most discrepant star, the mean value of $V_{WFPC2} - V_{ADCS93}$ becomes –0.004 ± 0.011 mag. We

then conclude that the WFPC2 And III F555W magnitudes have been reliably transformed to V. ADCS93 also observed And III in I rather than B and so no direct check of the F450W to B transformation is possible from these data. However, the relation between the $(B-V)_{WFPC2}$ and $(V-I)_{ADCS93}$ colors for the stars is consistent with that for metal-poor globular cluster red giants *if* the additional 0.055 mag zero-point adjustment found in Paper II is also applied in transforming the And III F450W magnitudes.

We have also searched the HST archive for observations of the ω Cen standard star field near in time to the And III observations. Photometry, using exactly the same procedures, including CTE correction, as outlined above, was obtained for 19 local photometric standards from Walker (1994) on a F450W, F555W pair of frames taken on 1999 June 14. The mean differences, between the WFPC2 photometry and that of Walker (1994), and their standard errors are –0.016 ± 0.007 for $V_{WFPC2}-V_{Walker}$ and +0.009 ± 0.012 for $(B-V)_{WFPC2}-(B-V)_{Walker}$, again after applying the additional 0.055 mag adjustment. These results then support the approach adopted in Paper II – use the H95 F555W to V transformation without modification and adjust the zero-point of the H95 F450W to B transformation by 0.055 mag in the sense of fainter B magnitudes and hence redder colors. Consequently, we have also adopted this approach for transforming the And III photometry to B and V. The resulting $(V, B-V)$ c-m diagram, again indicating the candidate variables, is shown in Fig. 3.

3. Results

3.1. The Color-Magnitude Diagrams of And III

In general, the c-m diagrams for And III presented in Figs. 2 and 3 bear a strong similarity to those for And I and And II (Paper II). The general morphology is that of an old metal-poor population – a relatively steep red giant branch and a significant number of (core-helium burning) horizontal branch (HB) stars which are predominantly red in color. With regard to the extent of contamination of these figures by non-And III members, the situation is clearly intermediate between that for And I and for And II (cf. Paper II). Since And III is also intermediate between And I and And II in its projected distance from the center of M31, the assertion that the principal contaminants of these c-m diagrams are (relatively metal-rich) M31 halo red giants is again supported (cf. Paper II). The degree of contamination of the principal sequences of And III by non-members is thus very limited and will not be considered further. The most striking difference between the c-m diagrams of Figs. 2 and 3 and the equivalent diagrams for And I and And II (Paper II) is the much less broad red giant branch for And III. In this respect and in terms of the HB morphology, the And III c-m diagram of Fig. 3 bears a strong resemblence to that for the Galactic dSph companion Draco. To illustrate this point, we show in Fig. 4 the Draco c-m diagram from Stetson (1979) at the same scale as Fig. 3. Aside from the larger sample in Fig. 3, the degree of similarity between the two c-m diagrams is self-evident. We shall elaborate on this similarity in

the subsequent discussion.

3.1.1. The Horizontal Branch Morphology

As is evident from Figs. 2 and 3, the horizontal branch morphology of And III is predominantly red. This is also the case for And I and And II (cf. Papers I and II) as it is for most of the Galaxy's dSph companions. In the c-m diagrams the red side of the And III HB is blended with the red giant branch and there is no clear distinction between the reddest of the core helium burning stars and the red giants at this luminosity. We take this to be a consequence of the photometric errors in the F450W–F555W colors (σ(F450W–F555W) $\approx$ 0.065 at the HB level, cf. Table 1) and of the lower sensitivity, relative to $B-V$, of F450W–F555W to differences in effective temperature.

In papers I and II we used an HB morphology index $i = b/(b+r)$ where b and r are the number of blue and red HB stars, respectively. We can readily use a similar index for And III although the process of comparing the And III index value with those for And I and II is complicated by the lower mean metallicity of And III (cf. Sect. 3.3). This lower abundance means both the red giant branch and the core-helium burning stars are notably bluer than for And I and II. Thus the red side of the color range used to quantify the number of red HB stars in And I and II (F450W–F555W = 0.60) is clearly inappropriate for And III. We adopt two approaches. First, as was done for And I and II, we constructed a color histogram for the stars in the magnitude interval corresponding to the horizontal branch, 24.85 $\leq$ F555W $\leq$ 25.25 in this case. This histogram shows a decline redward of F450W–F555W $\approx$ 0.50 and we adopt this as the limit beyond which red giants substantially outnumber red HB stars. We then take r as the number of stars in this magnitude interval with 0.35 $\leq$ F450W–F555W $\leq$ 0.50, yielding $r = 305$. For b we take the same magnitude interval but use –0.05 $\leq$ F450W–F555W $\leq$ 0.25 plus the two bluer, fainter stars. This gives $b = 30$ and thus $i_{III} = 0.09 \pm 0.02$ where the error is calculated assuming that b and r follow Poisson statistics. The subscript "*III*" is used to denote that this value comes from And III specific color limits. Excluding the candidate variables, the corresponding value of i_{III} is 0.08 $\pm$ 0.015.

The second approach used is to adopt the same color limits as were used to define the And I and II red HB star numbers and correct for the red giant branch star contamination by interpolation in the number of red giants above and below the horizontal branch. This approach yields $r = 266$ and thus with $b = 30$, $i = 0.10 \pm 0.02$ in good accord with the first estimate. For And I and And II we found values of 0.13 $\pm$ 0.01 and 0.18 $\pm$ 0.02, respectively, indicating that And III, despite being the lowest metallicity system (cf. Sect. 3.3), has the reddest HB morphology of the three Andromeda dSph companions studied in detail so far.

We can also compare the And III HB morphology directly with that of Draco, via the $(V, B-V)$ data of Figs. 3 and 4. For Draco we adopt r_{BV} as the number of stars with 19.85 $\leq V \leq$ 20.25 and 0.40 $\leq B-V \leq$ 0.60 (cf. Stetson (1979)). For b_{BV} we use the number of stars in the same magnitude interval, but with 0.00 $\leq B-V \leq$ 0.30 plus the three fainter stars with $(B-V) \approx 0.00$.

Then, for the Stetson (1979) data, $r_{BV} = 67$ and $b_{BV} = 9$ yielding $i_{BV} = 0.12 \pm 0.04$ for Draco. For And III, we adopt the same color limits for r_{BV} and a magnitude range (cf. Fig. 3) of $24.8 \leq V \leq 25.2$. This gives $r_{BV} = 224$ for the sample including the candidate variables. For b_{BV} we adopt the same magnitude interval, but use $-0.3 \leq B - V \leq 0.30$ plus the stars with $B - V \leq 0.25$ and $25.2 \leq V \leq 25.5$, once more including the candidate variables. Hence $b_{BV} = 20$ and $i_{BV} = 0.08 \pm 0.02$ for And III. This value is not appreciably altered if the candidate variables are excluded. It is also more correctly interpreted as an upper limit on the true value of i_{BV} for And III, as there are, for example, a further 80 or so probable red HB stars with $(B - V)$ colors between 0.65 and 0.70.

Comparison of this value of i_{BV} with that for Draco indicates that And III's HB morphology is probably somewhat redder than that of Draco. We will discuss the implications of this outcome below. Here it is worth noting that these results make the blue HB morphology of the Galactic dSph companion Ursa Minor look more and more unusual. Horizontal branch morphologies are now available for a number of M31 dSph companions (Paper I, II; this paper; Armandroff et al. 2002, in prep.) and there are no examples of HB morphologies even remotely like that of Ursa Minor. This is also the case for the Galactic dSph companions, as has been known for some time.

One further point deserves discussion here. In Paper I we showed that And I possesses a radial gradient in its HB morphology; the blue HB stars are found relatively more frequently beyond that dSph's core radius. Similar HB morphology radial gradients are also known to occur in at least two of the Galactic dSph companions (Paper I, Hurley-Keller et al. (1999), Majewski et al. (1999)). However, no such HB morphology gradient was found for And II (Paper II). It is therefore of interest to see whether an HB morphology gradient is present in And III. Caldwell et al. (1992) give the (geometric mean) core radius of And III as approximately $76''$ ($120''$ on the major axis, given that the ellipticity of And III is 0.6, Caldwell et al. (1992)). We have therefore divided our photometry sample, using the appropriate elliptical boundary, into "inside the core radius" and "outside the core radius" samples. The former contains 1338 stars with an average distance from the center of And III of $0.6\mathrm{r}_{core}$, while the latter sample contains 292 stars at an average radial distance of $1.3\mathrm{r}_{core}$. The most distant star is $2.2\mathrm{r}_{core}$ from the center. We also split the sample, again along an elliptical boundary, into two groups that contain approximately equal numbers of stars. This split occurs for a major axis radius of $82''$. In terms of r_{core}, the stars in the inner 50% sample have an average radial distance of $0.45\mathrm{r}_{core}$, while the outer 50% sample has an average radial distance of $1.0\mathrm{r}_{core}$.

For each of these samples we have calculated the And III HB morphology index i_{III} defined above. The resulting values are 0.08 ± 0.02 and 0.13 ± 0.05 for the inside and outside the core radius samples, respectively, and 0.07 ± 0.02 and 0.10 ± 0.02 for the inner and outer 50% samples. While these values hint at bluer HB morphology at larger distances from the center of And III, in fact the differences are not statistically significant: calculation of the T_2 statistic (cf. Paper I) indicates a $\sim$15% probability that the differences arise by chance alone. Thus And III joins And II in apparently lacking any HB morphology gradient, in contrast to And I.

3.1.2. Variable Stars

In Fig. 2 and 3 the majority of the stars that show discrepant colors or magnitudes between the two sets of observations lie on or near the horizontal branch. They are therefore most likely to be RR Lyrae variables, as was found to be the case for And I and II (Paper I, Paper II). To confirm this is also the case for And III, we have investigated a sample of these RR Lyrae candidate variables. This involved carrying out aperture photometry, in an identical fashion to that described above, including CTE corrections, for the candidate stars on the individual, as distinct from the combined, WFC frames. This leads, modulo measurements affected by cosmic rays, to two sets of 8 F450W and 4 F555W individual magnitudes, separated in time by ∼4.8 days. The total duration of each set is ∼0.4d, with the F450W observations occupying about 0.25d. These durations naturally limit the precision with which RR Lyrae like periods (i.e. typically 0.55d for ab-type RRs) can be determined.

The first step in the analysis was to plot the individual magnitudes against the epoch of mid-exposure to ascertain whether the star's brightness varied in a way consistent with timescales and amplitudes characteristic of RR Lyraes. The vast majority of the sample of stars investigated here did show such characteristics, and thus approximate periods were then estimated. In estimating these periods often a choice was required for the number of cycles between the two sets of observations. This was usually made considering the probable amplitude of variation. Further, frequently the F555W observations were also included in the period determination process, under the assumption that color variations are much smaller than those in brightness. Typical light curves from the sample of stars analyzed are shown in Fig. 5. These light curves, and others not shown, identify these stars as Type-ab RR Lyraes. It is important to remember, however, that we have not yet analyzed the data for all the candidate variables, nor have we yet conducted a more thorough search for all possible variables. As noted in Papers I & II, significant differences in color or magnitude in the data from the two sets of combined frames is a sufficient, but by no means necessary condition for detecting variable stars. We postpone to a subsequent paper a full investigation of the frequency of occurrence and properties of RR Lyrae stars on the horizontal branch of And III.

In Fig. 2 and 3 there are two candidate variables which are clearly brighter than the HB, yet which have colors that are not dissimilar to those of HB stars. Such stars, if they are indeed variables, are likely to be either Anomalous Cepheids (ACs) or Population II Cepheids.

Anomalous Cepheids, so-called because they do not obey the Period-Luminosity relations for either classical or Pop II cepheids (cf. Fig. 1, Zinn & Searle (1976)) are common in dSph galaxies – they are found in all such systems where variable star surveys have been carried out. On the other hand, they are extremely rare in the globular cluster population, with only one example known – V19 in NGC 5466 (Zinn & King 1982). The pulsation characteristics of ACs require masses in the range 1–2 $M_\odot$ and relatively low metallicities (e.g. Norris & Zinn (1975)). The first of these requirements then suggests that either ACs are stars of intermediate-age (age $\lesssim$ 5 Gyr, Demarque & Hirshfeld (1975)), or that they are older stars whose increased mass has been generated by mass

transfer in a binary system (e.g. Renzini et al. (1977)).

In contrast to ACs, Pop II cepheids are relatively common in the Galactic globular cluster population and are certainly rarer than ACs in dSphs (e.g. Nemec et al. (1994)). Pop II cepheids are understood as low mass (old) stars with low envelope masses that enter the instability strip either when evolving from a blue HB towards the AGB, or on blueward excursions from the AGB, or in the final blueward evolution at the end of the AGB phase.

We consider first the brighter variable candidate WF2-1398. Photometry of the individual data frames as described above for the candidate RR Lyrae stars confirms that this star is indeed a variable. The most likely period is 0.830d and the light curve for this period is shown in the upper panel of Fig. 6. For this light curve the (intensity weighted) mean F450W magnitude is approximately 23.5 and the amplitude is of order 1 mag. Using the distance modulus and reddening from Sect. 3.2, and assuming that for a star of this color F450W $\approx B$, we derive $< M_B > \approx$ –1.1 for this star. With this mean luminosity and period the star then lies squarely on the P-L relation for first overtone AC pulsators in Fig. 5 of Pritzl et al. (2002). Similarly, the amplitude and period are consistent with those for the ACs presented in Fig. 7 of Pritzl et al. (2002). We conclude therefore that this star is indeed an Anomalous Cepheid member of And III, joining those in And VI (Pritzl et al. 2002) as the first such stars discovered beyond the Galaxy and its companions. Given that ACs are common in the Galactic dSphs, the discovery of at least one AC in And III is perhaps not surprising, though a similar analysis to that carried out here did not reveal any promising AC candidates in either And I or And II. This may merely be a consequence of the lack, at the present time, of a detailed search for such variables in those dSphs (cf. Papers I, II).

The occurrence of ACs in And III, and their apparent absence in And I and II, confirms the trend from Galactic dSphs that such stars occur relatively more frequently in lower luminosity dSphs (e.g. Mateo et al. (1995)). Lower luminosity dSphs also have lower mean abundances and so this trend reinforces the result that, regardless of the mechanism(s) that generates anomalous cepheids (e.g. mass transfer binaries or single younger stars), a low metallicity stellar population is a necessary prerequisite for the existence of such stars.

The interpretation of the second candidate variable brighter than the HB, WF2-1710, is, unfortunately, not as straightforward though the individual frame data do indicate that the star is genuinely variable. Plausible light curves can be constructed for periods longer than ∼1 day, but shorter periods do not look viable. The light curve that results from an assumed period of 1.086d is shown in the lower panel of Fig. 6. From this light curve the mean F450W ($\approx B$) magnitude is approximately 24.55 corresponding to $< M_B > \approx$ –0.1. At this period and absolute magnitude, the star falls somewhat below the P-L relation for fundamental pulsator ACs in Fig. 5 of Pritzl et al. (2002). It is unclear how significant this discrepancy is given the lack of complete coverage of the light curve. The amplitude of variation is approximately 0.7 mag. This value and the assumed period are not obviously discrepant in Fig. 7 of Pritzl et al. (2002).

On the other hand, if the period is as long as 2.17d, which is equally consistent with the

observations, then this star is much more likely to be a Pop II Cepheid (BL Her star) than an AC. If this is the case then it would be somewhat unexpected for, at least in the Galactic globular clusters, Pop II cepheids are found only in those clusters with strong blue HB morphologies. Nemec et al. (1994) in their Table 4 list 20 BL Her stars in 10 Galactic globular clusters and the Harris catalog (Harris 1996) gives HB morphology indices (B–R)/(B+V+R) for 8 of these clusters. The average value of this morphology index is 0.88, on a scale where 1.00 is an entirely blue HB morphology and –1.00 is an entirely red HB. The other two clusters, ω Cen and NGC 6273, also have strong blue HBs: Harris (1996), for example, lists Dickens HB classifications for these clusters of 2 and 1, respectively, on a scale where 0 is a pure blue HB and 7 is pure red HB. Thus in Galactic globular clusters at least, it does appear that a strong blue HB morphology is required to produce BL Her type Pop II cepheids. Consequently, given the strong red HB morphology of And III, the occurrence of a Pop II cepheid in this system would be unexpected. We prefer then to interpret WF2-1710 as a second AC in And III, though further observations are clearly required to constrain more stringently the nature of this variable.

3.1.3. The Giant Branch Intrinsic Color Width

One of the characteristics that separates the Galactic dwarf spheroidal galaxies from the Galactic halo globular clusters (with the exception of ω Cen and perhaps also M22 and M54) is the presence in the dSphs of an intrinsic range in the abundance of the member stars. This abundance range can be revealed, given sufficiently accurate photometry of large samples of stars, by an observed red giant branch color width that is in excess of the width expected from the photometric errors alone. In Papers I and II we confirmed earlier suggestions, based on less precise ground-based photometry, of intrinsic giant branch color widths in the M31 dSphs And I and And II. Indeed, as discussed in Paper II, And I and And II have significantly different giant branch intrinsic color widths, with that for And II being substantially larger, despite the similar mean metallicities and luminosities of these two dSphs.

ADCS93 obtained ground-based V, I photometry of And III and used it, inter alia, to infer the presence of an intrinsic giant branch color width in this dSph. However, because they did not completely characterize their $V - I$ color errors, they were unable to fully quantify this intrinsic color width. By following the procedures outlined in Papers I and II, we can use our And III WFPC2 data to investigate this question further. The first step is to define a mean giant branch locus. This was done by fitting a low order polynomial to the stars in the interval $21.9 \leq$ F555W ≤ 23.9, excluding obvious outliers. Then, for each of the 60 stars in the interval $22.3 \leq$ F555W ≤ 23.3, again excluding outliers, we computed the difference between the F450W–F555W color of the star and the color of the mean giant branch at the F555W magnitude of the star. The mean of these differences is –0.001 mag (as expected) with a standard deviation σ_{obs}(F450W–F555W) = 0.048 mag. This value is not notably altered for modest changes in the magnitude range considered or by the inclusion or exclusion of the few outliers that lie near the giant branch. It is, however,

considerably smaller than the equivalent values for And I (0.068 mag using the corrected And I photometry of Paper II) and And II (0.12 mag, Paper II) for the same part of the red giant branch (between approximately 1.7 and 2.7 magnitudes above the horizontal branch). The difference between these residual color distributions on the red giant branch is illustrated in Fig. 7, where we have plotted the distributions for And I, II and III, normalized by the sample sizes of 114, 85 and 60 stars, respectively. In each case the photometric errors are comparable (cf. Papers I & II) so that the obvious apparent differences are a reflection of significant intrinsic differences.

Using the data of Table 1, the mean error in the And III F450W–F555W colors for 22.3 $\leq$ F555W $\leq$ 23.3 does not exceed 0.03 mag. Subtracting this value in quadrature then yields σ_{int}(F450W–F555W) = 0.038 mag for the And III giant branch. This confirms the results of ADCS93 in that the And III giant branch clearly does possess a small intrinsic color width. We defer to § 3.4 a discussion of the abundance spread implied by this intrinsic color width.

3.1.4. A Population of "Faint Blue Stars"?

In Papers I and II we noted that the And I and II c-m diagrams show a population of "faint blue stars" – stars with relatively blue colors ($B-V \lesssim 0.5$) that lie at least 0.5 mag fainter than the horizontal branch. It was not possible to dismiss these objects as artifacts of large color errors in subgiant photometry, and so they were considered a bone fide population in both dSphs. For And I, since there is no compelling evidence for any intermediate-age population (Mould & Kristian (1990), ADCS93, Armandroff (1994)), these faint blue stars were interpreted in Paper I as blue stragglers, analogous to those seen in many Galactic globular clusters. On the other hand, for And II there is evidence for an intermediate-age population (see the discussion in Sect. 3.5.2 of Paper II). Thus the faint blue stars in this dSph could consist of main sequence and main sequence turnoff stars as young as perhaps 1.5 Gyr, in addition to a blue straggler component (Paper II). Interestingly, these faint blue stars occur at a significantly higher frequency in And II than they do in And I (Paper II).

As for And III, there is some evidence from the c-m diagrams of Figs. 2 and 3 that a similar population of "faint blue stars" exists, although qualitatively the relative number of such stars appears smaller than for And II, for example. Further, since the lower mean metallicity of And III results in a bluer subgiant branch, it is possible that at least some of these And III "faint blue stars" are actually the result of large errors in the photometric colors of subgiant stars. In particular, based on the data of Table 1, at $V \approx 26$, the 1σ repeatability error in $B-V$ is approximately 0.18 mag, so that subgiants with $\gtrsim 2\sigma$ blueward errors will have $(B-V) \lesssim 0.5$ mag. Nevertheless, it seems unlikely that photometry errors could generate the stars with $V \approx 26$ and $(B-V) \lesssim 0.15$ visible in Fig. 3.

We can quantify the relative number of faint blue stars in And III by following the same procedures as in Paper II, in which the number of faint blue stars, hereafter FBS, is compared to

the number of subgiants, hereafter SG, with similar B magnitudes (since the completeness is set by the F450W data at these magnitudes). Noting that the HB in And III is approximately 0.1 mag fainter than that for And II, and that the reddenings are very similar, we take FBS for And III as the number of stars with $25.65 \leq V \leq 26.1$ and $(B-V) \leq 0.40$ mag, where the adopted color limit was chosen to minimize potential large color error subgiant contamination. There are 16 such stars with a mean B magnitude of 26.1. For SG we adopt the number of stars with $25.15 \leq V \leq 25.45$ and $0.60 \leq B-V \leq 0.95$; there are 89 such stars and their mean B magnitude is again 26.1, so that the completeness should be similar to that of the faint blue stars. The relative proportion of faint blue stars, $FBS/(FBS+SG)$, is then 0.15 ± 0.04 for And III; the error is calculated assuming Poisson statistics. The equivalent values for And I and And II (Paper II) are 0.21 ± 0.03 and 0.31 ± 0.04, respectively. Comparison with these values confirms the subjective impression that And III is relatively lacking in these faint blue stars, especially with respect to And II. Indeed, using the T_2 statistic (cf. Paper I) , there is a less than 1% chance that the And II and And III faint blue star proportions are drawn from the same underlying population.

Given that there is little evidence for an intermediate-age population in And III (ADCS93), it seems appropriate to conclude that these faint blue stars are predominantly blue stragglers analogous to those in the Galactic globular clusters.

3.2. The Distance of And III

The mean V magnitude of the 34 blue HB stars in Fig. 3 with $24.9 \leq V \leq 25.2$ and $0.05 \leq B-V \leq 0.45$ is 25.06 ± 0.015 (standard error of the mean). This value is unaltered for minor changes in the adopted color interval or if the candidate variables are excluded. We then adopt $V(\mathrm{HB}) = 25.06$ ± 0.04 for And III, where the error now includes uncertainty in the aperture corrections (±0.02) and in the zero-point/CTE corrections (±0.03). This apparent horizontal branch magnitude is intermediate between the values given in Paper II for And I (25.23 ± 0.04) and And II (24.93 ± 0.03).

To convert this value of V(HB) into a distance to And III, however, we need to adopt a reddening and a mean metal abundance. For the reddening, we follow Paper II and use the value of $E(B-V)$ given by the dust maps of Schlegel et al. (1998) at the location of And III. This value is $E(B-V) = 0.055 \pm 0.01$ so that $A_V = 0.18 \pm 0.03$ mag. The mean metallicity of And III is the subject of the next section; here we simply adopt the result <[Fe/H]> = –1.88 ± 0.11. In Papers I and II we adopted a distance scale specified by the relation $M_V(\mathrm{HB}) = 0.17[\mathrm{Fe/H}] + 0.82$. For consistency, we adopt this relation once more[2]. The absolute magnitude of the And III horizontal

[2]The relation is based on the horizontal branch models of Lee et al. (1990). More recent models (Demarque et al. 2000) have shown that the slope of the relation between M_V(RR) and [Fe/H] is dependant on abundance and that, at fixed [Fe/H], the value of M_V(RR) depends also on the horizontal branch morphology. Nevertheless, the new models suggest our adopted relation is not significantly in error, given the mean abundance and HB morphology of And III.

branch is then $M_V(\mathrm{HB}) = 0.50 \pm 0.02$ leading to $(m-M)_V = 24.56 \pm 0.05$ and $(m-M)_0 = 24.38 \pm 0.06$, or a distance of 750 ± 20 kpc on our adopted scale. This result is in extremely good agreement with the And III distance modulus, $(m-M)_0 = 24.4 \pm 0.2$, derived by ADCS93 from the I magnitude of the red giant branch tip. We note that the same (horizontal branch absolute magnitude, abundance) relation used here also underlies the ADCS93 modulus determination.

In Papers I and II the distances of the And dSph galaxies were compared to M31 using two somewhat different M31 distance moduli (on our adopted scale): 24.40 ± 0.13 based on RR Lyrae and field red giant data, and 24.64 ± 0.05 based on mean horizontal branch magnitudes for 8 M31 globular clusters (cf. Paper II). Recently, however, Durrell et al. (2001) have used the I magnitude of the red giant branch tip from a large sample of M31 halo red giants to derive an M31 distance modulus of $(m-M)_0 = 24.47 \pm 0.12$ (783 ± 43 kpc). The calibration employed by Durrell et al. (2001) is similar to that adopted here. This value is clearly close to one of our earlier adopted values. It is also consistent with the results of Holland (1998), who found $(m-M)_0 = 24.47 \pm 0.07$ from fits of theoretical giant branches to WFPC2 data for a number of M31 globular clusters. The Holland (1998) results are also on a scale similar to that used here. We will therefore adopt 780 ± 45 kpc as the distance to M31 for comparison with our And III results.

Adoption of this M31 distance then places And III 30 ± 50 kpc in front of M31 along the line-of-sight. The projected distance of And III from the center of M31 is $\sim$67 kpc and thus the true distance of And III from M31 is $R_{M31} \approx 75$ kpc. This value is intermediate between those for And I ($R_{M31} \approx 45$ kpc) and And II ($R_{M31} \approx 165$ kpc) and is comparable to the galactocentric distances of the nearer (excepting Sagittarius) of the Galaxy's dSph companions. For example, Draco and Sculptor have $R_G \approx 75$ and 79 kpc, respectively.

3.3. The Abundance of And III

To determine the mean abundance of And III we again follow the procedures outlined in Paper II, and fit standard globular cluster giant branches to the data of Fig. 3. Since the distance scale we employ is sensitive to abundance, this process is necessarily iterative, but convergence was rapid since an initial estimate of the mean And III abundance is available from ADCS93. The process involves calculating mean $B-V$ colors, excluding obvious outliers, for stars in a series of 0.2 mag wide V magnitude bins. There were six bins on the upper giant branch between $V = 22.3$ and $V = 23.5$ and two bins on the lower giant branch between $V = 25.3$ and $V = 25.7$ (i.e. fainter than the horizontal branch). Briefly, the lower giant branch bins offer the advantage of freedom from stars evolving from the horizontal branch and larger samples, but suffer from lower sensitivity to abundance, larger photometric errors and possibly more contamination from non-members. On the other hand, the upper giant branch offers better abundance sensitivity and smaller photometric errors even if the sample sizes are reduced. The possible influence of post-HB stars is also a potential concern at these luminosities but has not proved to be a problem (cf. Papers I and II).

The abundance corresponding to the mean color in each bin was determined by applying a calibration for that bin based on the standard globular cluster giant branches. These calibrations used the giant branch colors at the midpoint (in V) of each bin and the known abundances of the clusters taken from Armandroff (1989). These abundances are on the Zinn & West (1984) scale. Linear least squares fits were used for all except the three highest luminosity bins where quadratic fits were employed. The results of this process are illustrated in Fig. 8 which shows the mean $(B-V)$ colors and the standard globular cluster giant branches superposed on the And III data using $(m-M)_V = 24.56$ and $E(B-V) = 0.055$. The six higher luminosity bins give very consistent results (despite the small sample size in some cases) and yield <[Fe/H]> = –1.88 ± 0.04, where the uncertainty given reflects only the statistical uncertainty in the mean colors. The two lower luminosity bins are also consistent with each other and yield <[Fe/H]> = –1.72 ± 0.07, where again the uncertainty comes from just the statistical uncertainty in the mean colors. This latter abundance is 0.16 dex higher than the value derived from the upper giant branch. The difference between abundances derived from the upper and lower giant branches is reminiscent of that seen in the equivalent analyses in Papers I and II. For example, in Paper II the lower giant branch mean colors gave an abundance for And II that was 0.17 dex higher than the value determined from the upper giant branch. As was the case in Papers I and II, we prefer to adopt the mean And III abundance derived from the upper giant branch colors. This is primarily because the globular cluster standard giant branches are not as well determined at the lower luminosities, which combined with the strong abundance sensitivity to small changes in color at these luminosities, apparently results in this systematic offset.

The error in the mean abundance arising from the statistical uncertainty in the mean giant branch colors is, of course, not the only source of uncertainty. We have also to consider the effects of uncertainty in the $(B-V)$ zero-point, uncertainty in the distance modulus, and in the abundance calibration process itself. We take these to be ±0.03 mag, ±0.05 mag and ±0.05 dex, respectively, where the last value is a typical rms deviation about the least squares fits. The first two are equivalent to uncertainties in abundance of approximately 0.08 and 0.04 dex, respectively. Thus, while the uncertainty in the $(B-V)$ zero-point is the largest single contributor, it is by no means dominant. The combined uncertainty is 0.11 dex. The mean abundance of And III from our WFPC2 observations is then <[Fe/H]> = –1.88 ± 0.11 dex. This value is in excellent agreement with the earlier value, <[Fe/H]> = –2.0 ± 0.15, determined by ADCS93 from the $(V-I)$ colors of the And III red giant branch in ground-based data. And III thus retains its distinction as the dwarf with the lowest mean abundance among the known dSph companions to M31. With our mean abundance and the And III luminosity, $M_V = -10.35 \pm 0.1$, that follows from the apparent V magnitude measured by Caldwell et al. (1992) and the apparent modulus derived in the previous section, And III remains part of the well established correlation between mean abundance and luminosity for dSph galaxies (e.g. Caldwell (1999)).

One final point deserves mention. We have investigated whether there is any evidence for the presence of a radial abundance gradient in And III by computing mean giant branch colors for the

radially selected samples described in § 3.1.1. For both the samples inside and outside the core radius, and inside and outside the elliptical boundary which splits the total sample approximately in half, there is no evidence (or even suggestion) of any radial abundance gradient. The 3σ upper limit on any such gradient, within ∼1.3–1.5 core radii is approximately 0.4 dex. This lack of any abundance gradient in And III is consistent with the results for And I and And II (Papers I and II) and for the Galactic dSphs – in no dSph system has a radial abundance gradient been definitively established, though the Galactic dSph Fornax may be an exception (Saviane et al. 2000).

3.4. The Abundance Spread in And III

In § 3.1.3 we showed that the red giant branch of And III has a small, but nevertheless real, intrinsic color width. We now use the abundance calibration developed in the previous section to convert this intrinsic color width into an abundance distribution[3]. First, by applying the appropriate calibration to each of the 92 individual stars in the six upper giant branch V magnitude bins used for the mean abundance determination, we can generate 92 individual observed [Fe/H] values. The distribution of these observed [Fe/H] values is shown in Fig. 9. Also shown in this figure are the observed abundance distributions, derived in a similar fashion, for And I and And II from Paper II. The And III distribution is approximately gaussian in shape, and its narrow width stands in clear contrast to the broader distributions of And I and And II.

The And III distribution can be characterized in a number of ways: the standard deviation σ_{obs}([Fe/H]) is 0.15 dex, the interquartile range is 0.19 and the range of the central two-thirds of the sample is 0.32 dex. The apparent full abundance range is ∼0.6, from approximately –2.2 to –1.6 dex. The upper limit would appear to be relatively secure but the lower limit might be affected by the loss of sensitivity to metallicity of broad-band colors at low abundances, i.e. it is difficult to rule out the existence of And III stars with abundances below this limit. Nevertheless, as is readily apparent from Fig. 9, these And III values are notably smaller than the equivalent quantities for And I and And II (cf. Paper II). Indeed for And I and II, the contributions to the observed distributions from the photometric errors are negligible, and thus those distributions could be considered effectively intrinsic (cf. Paper II). However, this is not as obviously the case for And III.

Table 1 shows that for the magnitude range under consideration, the photometric errors in the F450W–F555W colors are 0.026 mag or less. We conservatively adopt σ_{err}(F450W–F555W) = 0.03 mag. Given the slope of the F450W–F555W to $B-V$ transformation and the mean color of the red giants in the sample, this adopted photometric error corresponds to $\sigma_{err}(B-V) = 0.038$ mag, or using the mean slope of the abundance calibrations, to σ_{err}([Fe/H]) = 0.10 dex. Subtracting

[3]The lack of evidence for any intermediate-age population in And III allows this interpretation (cf. Carina, Smecker-Hane et al. (1999) and Leo I, Gallart et al. (1999)).

this value in quadrature from the observed standard deviation then gives σ_{int}([Fe/H]) = 0.12 for the And III intrinsic abundance distribution.

This value is somewhat smaller than the limits given by ADCS93 who found $0.16 \leq \sigma_{int}([Fe/H]) \leq 0.24$ from their ground-based V and I photometry. Taken at face value, the dispersion derived here is one of the smallest intrinsic abundance dispersions known for a dSph galaxy (cf. Mateo (1998)). However, we caution against placing too much weight on the exact value of the And III abundance dispersion, though it is evident from Fig. 9 that σ_{int}([Fe/H]) for And III is not large. Specifically, as noted above, the colors of old red giants are certainly metallicity dependant, but as the abundance is lowered below –2.3, or thereabouts, the dependance on color is much reduced. Thus, it is potentially possible that a significant abundance range may be hidden by the color degeneracy of very metal-poor red giant stars. Nevertheless, Fig. 9 does not suggest this is obviously the case for And III.

However, amongst the lower luminosity Galactic dSphs, i.e. those most comparable in luminosity to And III, there are clear disparities between inferences from c-m diagrams and from spectroscopy of individual stars. For example, for Draco (cf. Fig. 4), Ursa Minor, Sextans and Carina, there is only limited evidence for intrinsic giant branch color widths in any of these systems (Stetson 1979; Olszewski & Aaronson 1985; Suntzeff 1993; Smecker-Hane et al. 1994). This is due at least in part to the relatively small numbers of red giants in these systems, and to the difficulty of deciding the membership, based on photometry alone, of potential members that deviate from the principal sequences. For the case of Carina it appears that the age range present in this dSph may have conspired with a metallicity range to produce the relatively narrow upper giant branch (Smecker-Hane et al. 1999). However, in all cases spectroscopic observations indicate the presence of significant abundance ranges in these systems. Suntzeff (1993) gives σ_{int}([Fe/H]) $\approx$ 0.30 for Draco and $\approx$0.27 for Ursa Minor, while Suntzeff et al. (1993) give σ_{int}([Fe/H]) = 0.19 $\pm$ 0.02 for Sextans and Smecker-Hane et al. (1999) give σ_{int}([Fe/H]) $\approx$ 0.25 for Carina.

These values all exceed our photometric value of σ_{int}([Fe/H]) for And III and suggest that a spectroscopic survey of member red giants is needed to fully constrain the And III abundance distribution. In this context it is worth noting that for And II, where σ_{int}([Fe/H]) is evidently large, the photometric abundance distribution (Paper II) agrees well with spectroscopic determination (Côté et al. 1999). If the relatively narrow And III abundance distribution is confirmed via spectroscopy, then the implication would be that And III retained relatively little of the enrichment products generated during its evolutionary history. This appears also to be the case for the Galactic dSph Leo I where Gallart et al. (1999) have inferred a narrow abundance distribution from their analysis of a WFPC2 based c-m diagram, despite the extended star formation history of this dwarf. These results underline the fact that the intrinsic abundance distribution is a vital component in any analysis of the evolutionary history of dwarf galaxies.

3.5. The Age(s?) of And III

The occurrence of blue HB stars and RR Lyrae variables in the c-m diagrams of And III (cf. Fig. 2, Fig. 3) unambiguously indicates the presence of a population in this dSph whose age is essentially the same as that of the Galactic halo globular clusters. This result comes as no surprise since in every dSph system where sufficient data exists, there is evidence for the presence of such old (age $\geq$ 10 Gyr) populations. Given the results of Held et al. (2001), this statement now also includes the dSph Leo I, despite its dominant comparatively young population (e.g. Gallart et al. (1999)). For And III, since the BHB stars are $\sim$10% of the total HB population (cf. § 3.1.1), this percentage can be taken as a lower limit on the size of the old population in And III. On the other hand, ADCS93 have demonstrated that And III does not contain any significant population with ages considerably less than $\sim$10 Gyr. Based on the presence of a small number of stars brighter than the red giant branch tip in a field-subtracted I-band luminosity function, these authors concluded that the And III population fraction with ages between $\sim$3 and 10 Gyr was only 10 $\pm$ 10 per cent. There was no indication of any yet younger stars.

Nevertheless, despite the presence of a limited number of BHB stars, the bulk of the And III HB population lies to the red of the instability strip, and is thus potentially of younger age than most of the Galactic globular clusters. The actual age difference, however, is not easily quantified. As discussed in Rey et al. (2001) (see also Lee et al. (1999, 2001)), the latest synthetic HB models suggest an increased sensitivity of HB morphology to age, as compared to earlier models (e.g. Lee et al. (1994)). Indeed as Fig. 9 of Rey et al. (2001) suggests the age difference required for a significant HB morphology shift is now approximately half that implied by the earlier models. Using this figure together with the mean And III abundance of $<$[Fe/H]$>$ $\approx$ –1.9 (cf. § 3.3), the dominant red morphology of the And III horizontal branch suggests that the bulk of the population in this dSph is $\sim$3 to 3.5 Gyr younger than the Galactic inner halo globular clusters, and $\sim$2 Gyr younger than those globular clusters with R_{GC} exceeding 8 kpc (cf. Fig. 9 of Rey et al. (2001)). This age difference is consistent with the results of ADCS93 who found only a small number of stars above the And III red giant branch tip and thus inferred a small intermediate-age population fraction: only if the age difference was greater would larger numbers of such stars be expected.

What evidence is there to support this "age is the second parameter" interpretation of the And III HB morphology? First, there is the consistency between red HB morphologies and the "young" mean ages determined from main sequence turnoff photometry for a number of Galactic dSphs. As noted in the Introduction, for Carina, Leo I, Leo II and Fornax, there is a direct observed connection, via main sequence turnoff photometry, between a mean age younger than that of the Galactic globular clusters, and a red HB morphology. This age – horizontal branch morphology connection is also reinforced by Ursa Minor where the strong blue HB morphology in this dSph goes with an age indistinguishable from that of the globular clusters of the inner Galactic halo (Olszewski & Aaronson 1985; Mighell & Burke 1999). Second, recent data for pairs of Galactic globular clusters with similar abundances but different HB morphologies are revealing age differences from main sequence turnoff photometry (e.g. Green & Norris (1990); Stetson et al.

(1999); Bellazzini et al. (2001); Rey et al. (2001) that are consistent with those inferred from the new HB models (e.g. Rey et al. (2001); Catelan et al. (2001)). Thus, while acknowledging that for Galactic globular clusters additional parameters such as cluster density, rotation, etc, may also influence HB morphology, the available evidence does support our interpretation of the And III HB morphology in terms of a younger age. Confirmation of this interpretation via photometry of the And III main sequence turnoff is, unfortunately, beyond currently available resources.

In § 3.1.1 we argued that the And III HB morphology is similar to, or even perhaps somewhat redder than, the HB morphology of Draco. Consequently, as for And III, we infer from Fig. 9 of Rey et al. (2001) that the dominant population of Draco should be ∼3 Gyr younger than the majority of Galactic globular clusters. The results of Grillmair et al. (1998), however, appear to contradict this assertion. These authors, using WFPC2 observations that reach well below the main sequence turnoff in Draco, find that the age of the dSph is nominally 1.6 ± 2.5 Gyr *older* than the Galactic halo globular clusters M68 and M92. Modulo possible calibration uncertainties (cf. § 3.2 of Grillmair et al. (1998)) and uncertainties in the cluster fiducials against which the comparison was made (cf. the discussion in § 1 of Rey et al. (2001)), the Grillmair et al. (1998) result is $\sim 1.8\sigma$ away from our HB morphology based age for Draco. It is difficult to decide the significance of this contradiction. As Grillmair et al. (1998) themselves admit, the WFPC2 Draco observations are not of the highest quality and their sample of turnoff stars is limited by WFPC2's small field. A new investigation of this question based on high quality data, perhaps obtained with the new generation 8-10m class telescopes, is clearly warranted.

Two other recent papers have also investigated the star formation history of Draco. Aparicio et al. (2001) have used data obtained from a 2.5m telescope in their analysis. While these data cover a wide field and thus provide a large sample of Draco stars, the precision of the photometry in the vicinity of the main sequence turnoff and fainter is limited. This restricts the degree to which they can constrain the age of the bulk of the population in Draco. They confirm that the bulk of the stars are older than 10 Gyr, but cannot distinguish if "the most conspicuous population is 12–13.5 or 13.5–15 Gyr old" (Aparicio et al. 2001). The other paper is that of Dolphin (2002), which analyses the same WFPC2 data set as Grillmair et al. (1998). Despite the use of sophisticated c-m diagram modelling techniques, Dolphin (2002) concludes only that the bulk of the star formation in Draco occurred at early times (ages ≥11 Gyr); it is not possible to establish whether this corresponds to the age of the Galactic globular clusters, or not. Thus we conclude that an age for Draco ∼3 Gyr younger than that of the Galactic globular clusters cannot be conclusively ruled out at this time.

4. Discussion

With the analysis of our And III observations, we now have c-m diagrams for all three of the original (cf. van den Bergh (1972, 1974)) dSph companions to M31. These c-m diagrams are shown in Fig. 10. All three systems have dominant red HB morphologies which we have interpreted as indicating the presence of substantial populations in each dSph that are younger than the

Galactic globular clusters (cf. § 3.5, Paper I, Paper II). Only And II, however, possesses a definite intermediate-age population (see Paper II and references therein).

The strong red HB morphologies for the And dSphs are reminiscent of the dominant red HB morphologies found among the Galactic dSph systems, where the blue HB of Ursa Minor is the only counter example among the Galaxy's nine dSph companions. In this respect then, the two sets of dSph companions are similar. They are also similar in that they obey the same relations between mean metallicity, luminosity, central surface brightness and length scale (e.g. Caldwell et al. (1992); Caldwell (1999)). The major *difference* between the two systems is the comparative lack of intermediate-age populations in the M31 dSphs. Among the Galaxy's companions, Fornax, Leo I and Carina, for example, all have significant populations with ages less than a few Gyr, or even younger, whereas such populations are completely unknown among the M31 dSph companions. This statement can be extended to include the recently discovered systems And V, VI and Cas (And VII), since ground-based c-m diagrams for the red giant branch in these systems have not revealed any prominent upper-AGB star populations (Armandroff et al. 1998, 1999; Hopp et al. 1999; Grebel & Guhathakurta 1999). Such upper-AGB stars are, however, seen in the c-m diagrams of two M81 Group dSphs, neither of which is obviously associated with any large galaxy (Caldwell et al. 1998). It then seems likely that we are seeing an environmental effect in the comparative lack of intermediate-age stars in the M31 dSphs. Some process or processes (e.g. ram pressure stripping in a hot gaseous corona, and/or supernovae-driven galactic winds and/or a high-UV flux from the bulge of M31) seems to have affected the M31 dSphs, removing their gas and largely terminating their star formation ∼10 Gyr ago. Evidently this process or processes wasn't as strong for the Galaxy and its dSph companions.

In this context it is worth recalling that among the Galactic dSphs, there is a tendency for the more distant systems to have larger and younger intermediate-age populations (e.g.van den Bergh (1994)). Although the size of any intermediate-age population in the M31 dSphs is less than that of most of the Galaxy's dSph companions, there is a suggestion here of a similar radial trend. Of the three M31 systems studied so far, it is the most radially distant dSph And II that contains a definite intermediate-age population. Further, the intermediate distance system And III has, based on its redder HB morphology despite a lower mean abundance, a mean age somewhat younger than that of the innermost system And I. It will be interesting to see if this possible trend is confirmed when similar analyses become available for the other M31 dSphs – And V, And VI and Cas (And VII). The latter two objects are of particular interest in this context since their distances from the center of M31 exceed that of And II.

One further point deserves mention. As noted in the Introduction, Blitz & Robishaw (2000) have claimed an association between an H I cloud and And III.[4] The gas cloud has a heliocentric radial velocity of –341 ± 6 km s^{-1}, which is in good agreement with the optical velocity of And III (V_r = –351 ± 9 km s^{-1}, Côté et al. (2000)). If the cloud is at approximately the same distance

[4]See also the additional information contained in the *Note added in proof* in Blitz & Robishaw (2000).

as And III, then it has an H I mass of $\sim 10^5$ $M_\odot$ and is centered about 3.7 kpc from the center of And III. Given that the (geometric mean) limiting radius of And III is approximately 1.35 kpc (Caldwell et al. 1992), there is little overlap between the H I cloud and the optical extent of the galaxy. Clearly, as the color-magnitude diagrams of Figs. 2 and 3 show, the apparent presence of the H I cloud has had little influence on the star formation history of And III – there is simply no indication of any young stars in this dSph.

This situation is reminiscent of those for the dSphs Leo I, Sextans and Sculptor. All three dSphs have claimed associations with H I clouds or complexes (Blitz & Robishaw (2000), but see also Young (2000); Carignan et al. (1998), Carignan (1999)). The bulk of the stellar population of Leo I has an age in the range of 1–7 Gyr, with few, if any, stars significantly younger (Gallart et al. 1999), while Sextans and Sculptor have no significant populations younger than a few Gyrs or more (Mateo et al. 1991; Hurley-Keller et al. 1999). Thus, as for And III, the apparent presence of nearby H I has not had any recent influence on the star formation in these systems. This circumstance contrasts with that for the dSph/dIrr systems LGS 3 and Phoenix. Here the H I is coincident (LGS 3, Young & Lo (1997)) or near-coincident (Phoenix, Gallart et al. (2001); St-Germain et al. (1999)) with the optical galaxy, and both dwarfs have had star formation within the past $\sim$100 Myr or so (e.g. Holtzman et al. (2000); Aparicio et al. (1997); Miller et al. (2001)). Apparently, assuming the H I/dSph associations are real, it seems that possible evolutionary outcomes for such gas clouds include no star formation at all, star formation ceasing at a variety of past times, and on-going star formation. The individual outcomes are presumably dependant on the density and dark matter content of the clouds, on the potential-well depth of any associated dwarf galaxy and on environmental influences.

The authors are grateful to Dr. Bart Pritzl for helpful input to the discussion of the variable star candidates. This research was supported in part by NASA through grant number GO-07500 from the Space Telescope Science Institute, which is operated by AURA, Inc., under NASA contract NAS 5-26555.

REFERENCES

Aparicio, A., Gallart, C., & Bertelli, G. 1997, AJ, 114, 680

Aparicio, A., Carrera, R., & Martínez-Delgado, D. 2001, AJ, 122, 2524

Armandroff, T. E. 1989, AJ, 97, 375

Armandroff, T. E. 1994, in An ESO/OHP Workshop on Dwarf Galaxies, ed. G. Meylan & P. Prugniel (Garching: ESO), 211

Armandroff, T. E., Da Costa, G. S., Caldwell, N., & Seitzer, P. 1993, AJ, 106, 986 (ADCS93)

Armandroff, T. E., Davies, J. E., & Jacoby, G. H. 1998, AJ, 116, 2287

Armandroff, T.E., Jacoby, G. H., & Davies, J. E. 1999, AJ, 118, 1220

Bellazzini, M., Fusi Pecci, F., Ferraro, F. R., Galleti, S., Catelan, M., & Landsman, W. B. 2001, AJ, 122, 2569

Blitz, L., & Robishaw, T. 2000, ApJ, 541, 675

Caldwell, N., Armandroff, T. E., Da Costa, G. S., & Seitzer, P. 1998, AJ, 115, 535

Caldwell, N. 1999, AJ, 118, 1230

Caldwell, N., Armandroff, T. E., Seitzer, P., & Da Costa, G. S. 1992, AJ, 103, 840

Carignan, C. 1999, Publ. Astron. Soc. Aust., 16, 18

Carignan, C., Beaulieu, S., Côté, S., Demers, S., & Mateo, M. 1998, AJ, 116, 1690

Catelan, M., Bellazzini, M., Landsman, W. B., Ferraro, F. R., Fusi Pecci, F., & Galleti, S. 2001, AJ, 122, 3171

Côté, P., Oke, J. B., & Cohen, J. G. 1999, AJ, 118, 1645

Côté, P., Mateo, M., Sargent, W. L. W., & Olszewski, E. W. 2000, ApJ, 537, L91

Da Costa, G. S. 1998, in Stellar Astrophysics for the Local Group, ed. A. Aparicio, A. Herrero, & F. Sánchez, (Cambridge, Cambridge Univ. Press), 351

Da Costa, G. S., Armandroff, T. E., Caldwell, N., & Seitzer, P. 1996, AJ, 112, 2576 (Paper I)

Da Costa, G. S., Armandroff, T. E., Caldwell, N., & Seitzer, P. 2000, AJ, 119, 705 (Paper II)

Demarque, P., & Hirshfeld, A. W. 1975, ApJ, 202, 346

Demarque, P., Zinn, R., Lee, Y.-W., & Yi, S. 2000, AJ, 119, 1398

Dolphin, A. E. 2000, PASP, 112, 1397

Dolphin, A. E. 2002, MNRAS, in press (astro-ph/0112331)

Durrell, P. R., Harris, W. E., & Pritchet, C. J. 2001, AJ, 121, 2557

Gallart, C., Freedman, W. L., Aparicio, A., Bertelli, G., & Chiosi, C. 1999, AJ, 118, 2245

Gallart, C., Martínez-Delgado, D., Gómez-Flechoso, M. A., & Mateo, M. 2001, AJ, 121, 2572

Grebel, E. K. 1999, in IAU Symp. 192, The Stellar Content of Local Group Galaxies, ed. P. Whitelock & R. Cannon (San Francisco: ASP), 17.

Grebel, E., & Guhathakurta, P. 1999, ApJ, 511, L101

Green, E. M., & Norris, J. E. 1990, ApJ, 353, L17

Grillmair, C. J., et al. 1998, AJ, 115, 144

Harris, W. E. 1996, AJ, 112, 1487

Held, E. V., Clementini, G., Rizzi, L., Momany, Y., Saviane, I., & Di Fabrizio, L. 2001, ApJ, 562, L39

Holland, S. 1998, AJ, 115, 1916

Holtzman, J. A., Burrows, C. J., Casertano, S., Hester, J. J., Trauger, J. T., Watson, A. M., & Worthey, G. 1995, PASP, 107, 1065 (H95)

Holtzman, J. A., Smith, G. H., & Grillmair, C. 2000, AJ, 120, 3060

Hopp, U., Schulte-Ladbeck, R. E., Greggio, L. & Mehlert, D. 1999, A&A, 342, L9

Hurley-Keller, D., Mateo, M., & Nemec, J. 1998, AJ, 115, 1840

Hurley-Keller, D., Mateo, M., & Grebel, E. K. 1999, ApJ, 523, L25

Lee, Y.-W., Demarque, P., & Zinn, R. 1990, ApJ, 350, 155

Lee, Y.-W., Demarque, P., & Zinn, R. 1994, ApJ, 423, 248

Lee, Y.-W., Yoon, S.-J., Lee, H.-C., & Woo, J.-H. 1999, in ASP Conf. Proc. 192, Spectrophotometric Dating of Stars and Galaxies, ed. I. Hubeny, S. Heap, & R. Cornett (San Francisco: ASP), 185

Lee, Y.-W., Yoon, S.-J., Rey, S.-C., & Chaboyer, B. 2001, in ASP Conf. Proc. 245, Astrophysical Ages and Time Scales, ed. T. von Hippel, C. Simpson, & N. Manset (San Francisco: ASP), 343

Majewski, S. R., Siegel, M. H., Patterson, R. J., & Rood, R. T. 1999, ApJ, 520, L33

Mateo, M. 1998, ARA&A, 36, 435

Mateo, M., Nemec, J., Irwin, M., & McMahon, R. 1991, AJ, 101, 892

Mateo, M., Fischer, P., & Krzeminski, W. 1995, AJ, 110, 2166

Mighell, K. J., & Burke, C. J. 1999, AJ, 118, 366

Mighell, K. J., & Rich, R. M. 1996, AJ, 111, 777

Miller, B. W., Dolphin, A. E., Lee, M.-G., Kim, S.-C., & Hodge, P. 2001, ApJ, 562, 713

Mould, J., & Kristian, J. 1990, ApJ, 354, 438

Nemec, J. M., Nemec, A. F. L., & Lutz, T. E. 1994, AJ, 108, 222

Norris, J., & Zinn, R. 1975, ApJ, 202, 335

Olszewski, E. W., & Aaronson, M. 1985, AJ, 90, 2221

Pritzl, B. J., Armandroff, T. E., Jacoby, G. H., & Da Costa, G. S. 2002, AJ, submitted

Renzini, A., Mengel, J. G., & Sweigart, A. V. 1977, A&A, 56, 369

Rey, S.-C., Yoon, S.-J., Lee, Y.-W., Chaboyer, B., & Sarajedini, A. 2001, AJ, 122, 3219

Saviane, I., Held, E. V., & Bertelli, G. 2000, A&A, 355, 56

Schlegel, D. J., Finkbeiner, D. P., & Davis, M. 1998, ApJ, 500, 525

Smecker-Hane, T. A., Stetson, P. B., Hesser, J. E., & Lehnert, M. D. 1994, AJ, 108, 507

Smecker-Hane, T. A., Stetson, P. B., Hesser, J. E., & VandenBerg, D. A. 1996, in From Stars to Galaxies: The Impact of Stellar Physics on Galaxy Evolution, ed. C. Leitherer, U. Fritze-von Alvensleben & J. Huchra (ASP: San Francisco), ASP Conf. Ser., 98, 328

Smecker-Hane, T. A., Mandushev, G. I., Hesser, J. E., Stetson, P. B., Da Costa, G. S., & Hatzidimitriou, D. 1999, in ASP Conf. Proc. 192, Spectrophotometric Dating of Stars and Galaxies, ed. I. Hubeny, S. Heap, & R. Cornett (San Francisco: ASP), 159

Stetson, P. B. 1979, AJ, 84, 1149

Stetson, P. B., Hesser, J. E., & Smecker-Hane, T. A. 1998, PASP, 110, 533

Stetson, P. B., et al. 1999, AJ, 117, 247

St-Germain, J., Carignan, C., Côté, S., & Oosterloo, T. 1999, AJ, 118, 1235

Suntzeff, N. 1993, ASP Conf. Proc. 48, The Globular Cluster–Galaxy Connection, ed. G. H. Smith & J. P. Brodie (San Francisco: ASP), 167

Suntzeff, N. B., Mateo, M., Terndrup, D. M., Olszewski, E. W., Geisler, D., & Weller, W. 1993, ApJ, 418, 208

van den Bergh, S. 1972, ApJ, 171, L31

van den Bergh, S. 1974, ApJ, 191, 271

van den Bergh, S. 1994, ApJ, 428, 617

Walker, A. R. 1994, PASP, 106, 828

Whitmore, B., Heyer, I., & Casertano, S. 1999, PASP, 111, 1559

Young, L. M. 2000, AJ, 119, 188

Young, L. M., & Lo, K. Y. 1997, ApJ, 490, 710

Zinn, R., & King, C. R. 1982, ApJ, 262, 700

Zinn, R., & Searle, L. 1976, ApJ, 209, 734

Zinn, R., & West, M. J. 1984, ApJS, 55, 45

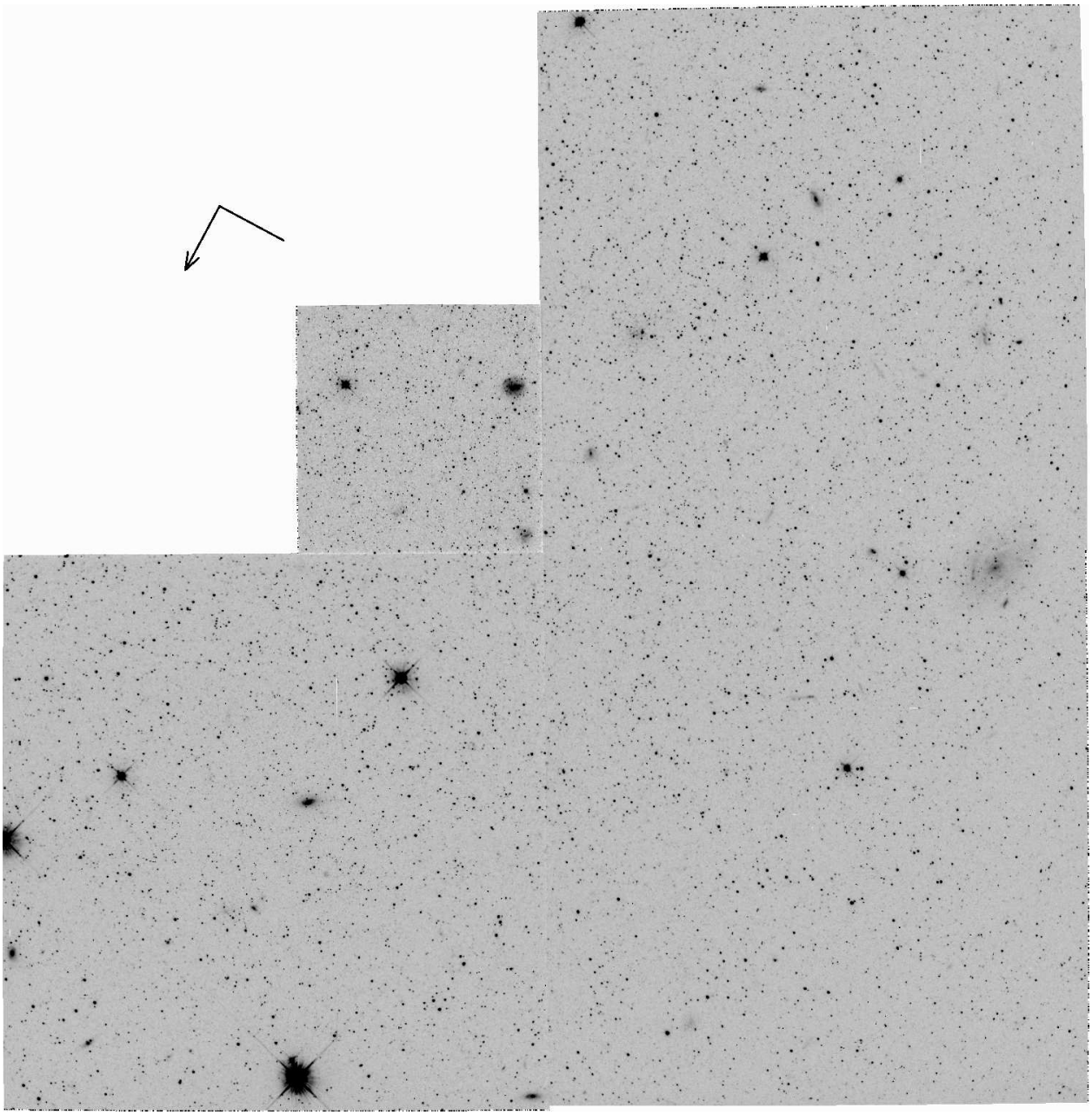

Fig. 1.— A mosaic of the And III WFPC2 field made from the combination of four 1200 s F555W exposures. North is indicated by the direction of the arrow and East by the line. Both indicators are 10″ in length.

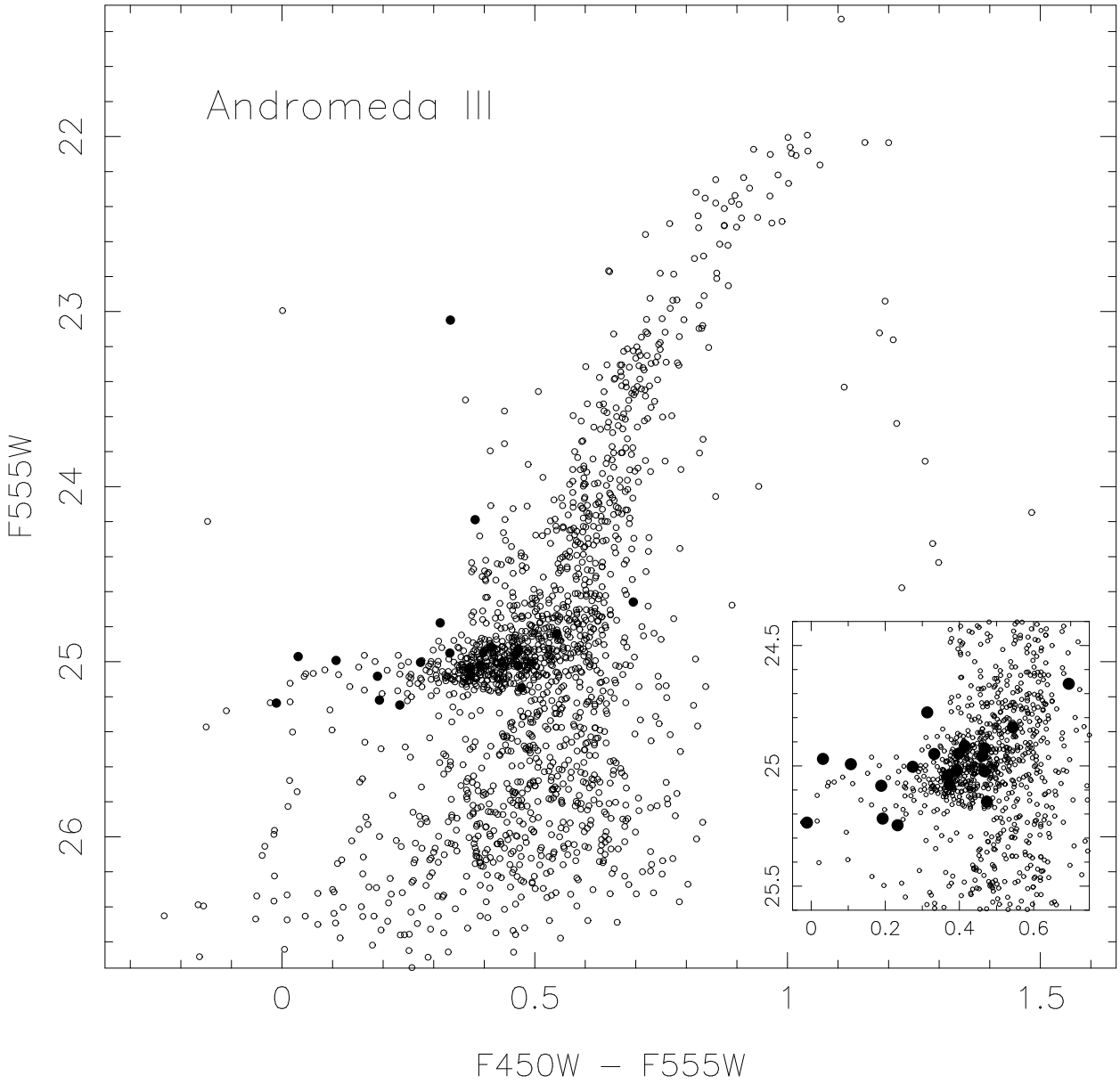

Fig. 2.— A color-magnitude diagram for Andromeda III. The photometry is on the F450W, F555W system of Holtzman et al. (1995). Charge transfer efficiency corrections from Whitmore et al. (1999) have been applied. The filled symbols are stars which show large magnitude or color differences between the two sets of observations. Most are likely to be And III variable stars. The insert box enlarges a region around the horizontal branch.

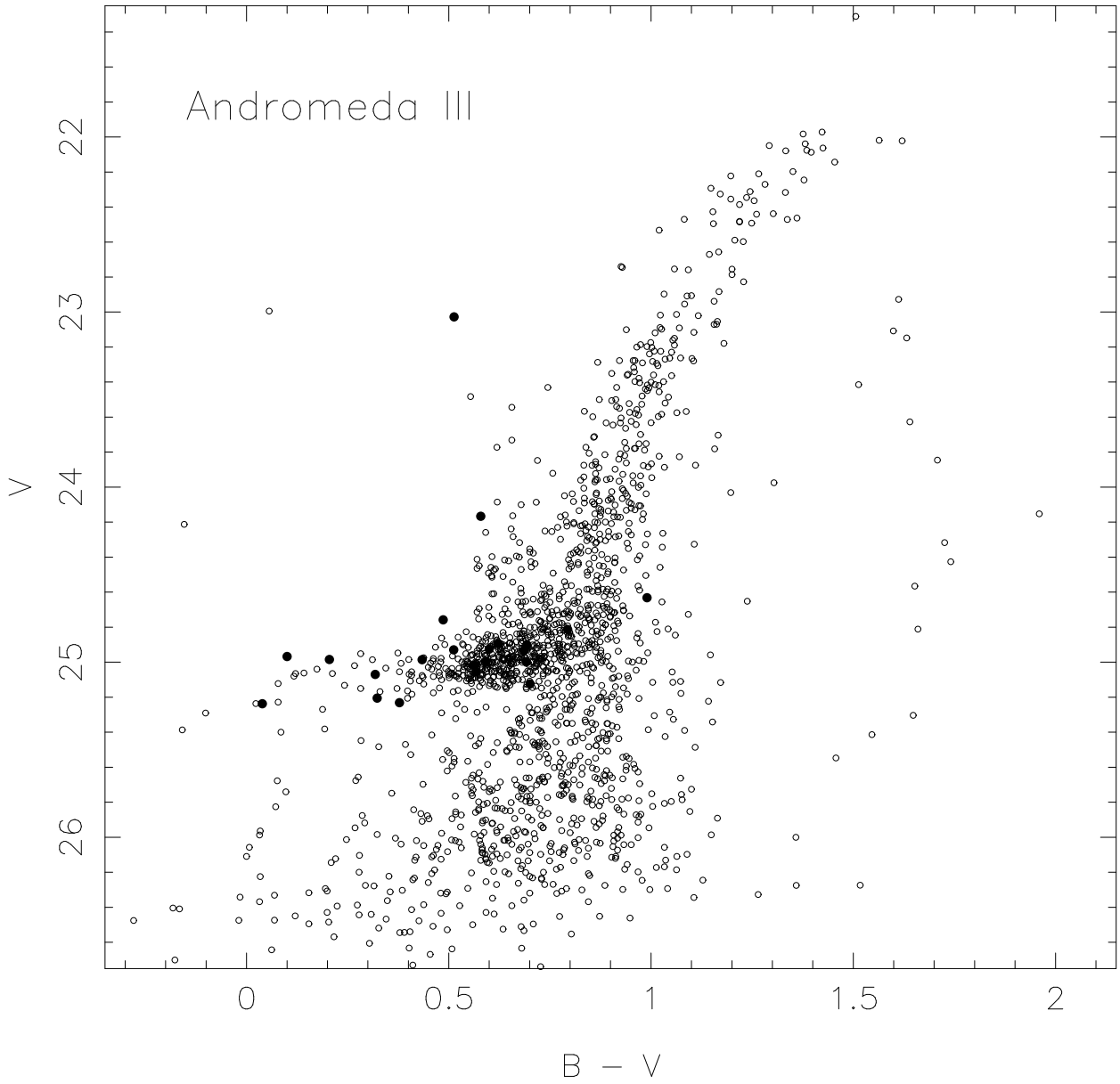

Fig. 3.— A color-magnitude diagram for Andromeda III on the standard B, V system. The candidate variable stars are plotted as filled symbols.

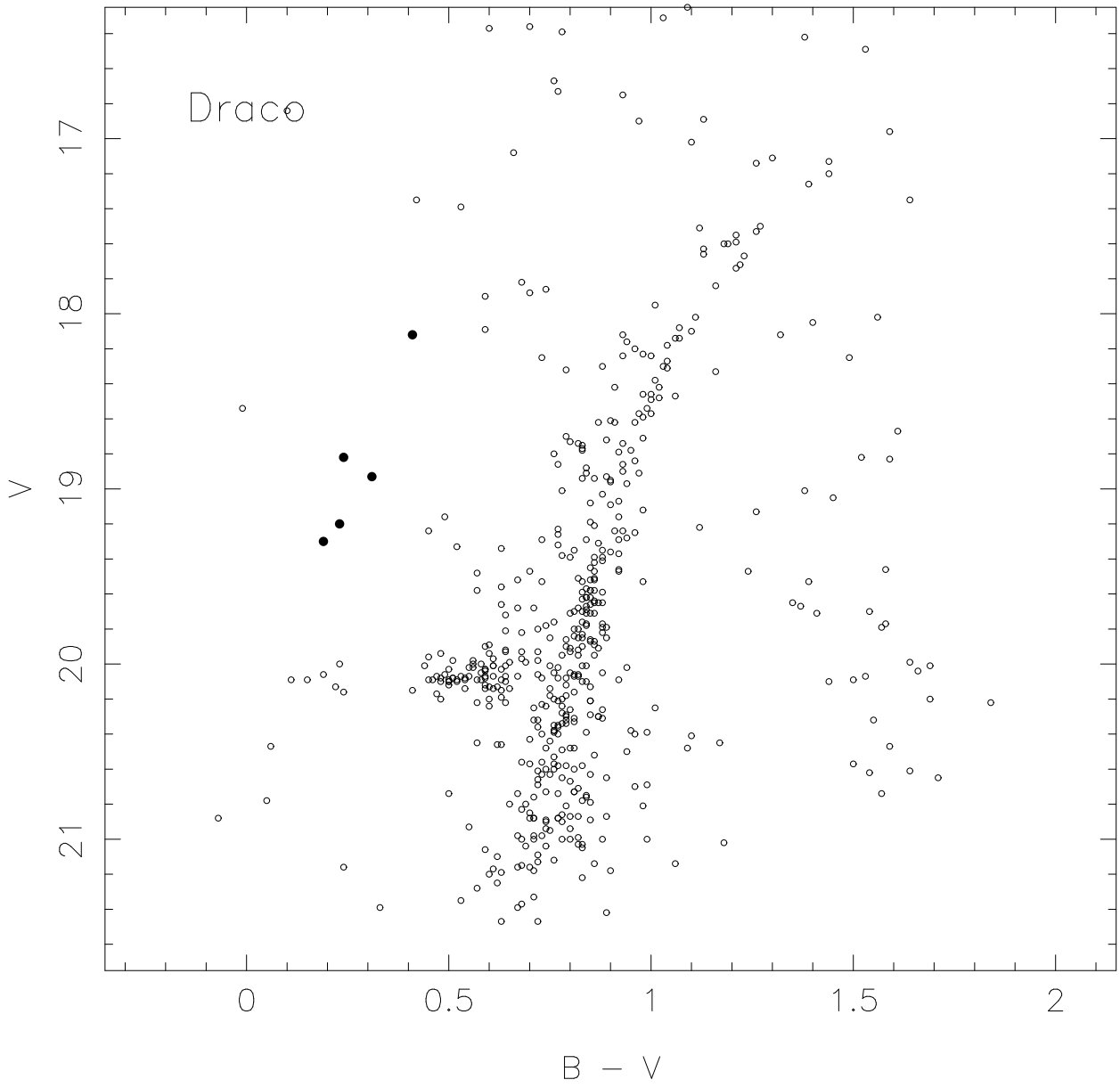

Fig. 4.— A color-magnitude diagram for the Galactic dSph Draco using the photometry of Stetson (1979). The filled symbols are Draco Anomalous Cepheid variables plotted at values of $< V >$ and $< B > - < V >$ tabulated by Pritzl et al. (2002).

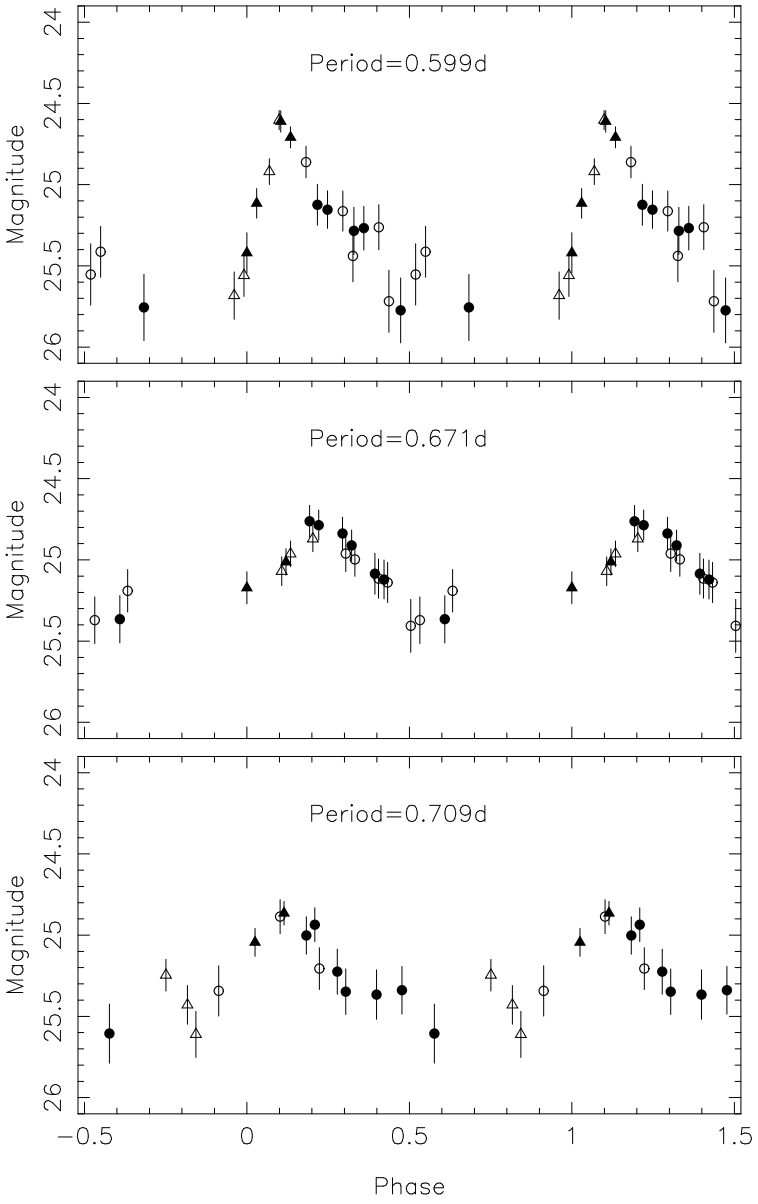

Fig. 5.— Light curves for 3 And III RR Lyrae variables. These stars come from the candidate variables identified in Figs. 2 and 3. Two cycles are plotted for each star, with the filled and unfilled symbols representing the two sets of observations. F450W magnitudes are shown as circles while F555W magnitudes are shown as triangles. A constant F450W–F555W color of 0.20 mag has been assumed to place the F555W observations with those for F450W. The error bars are those from photon statistics and the period adopted for each star is given in the panels.

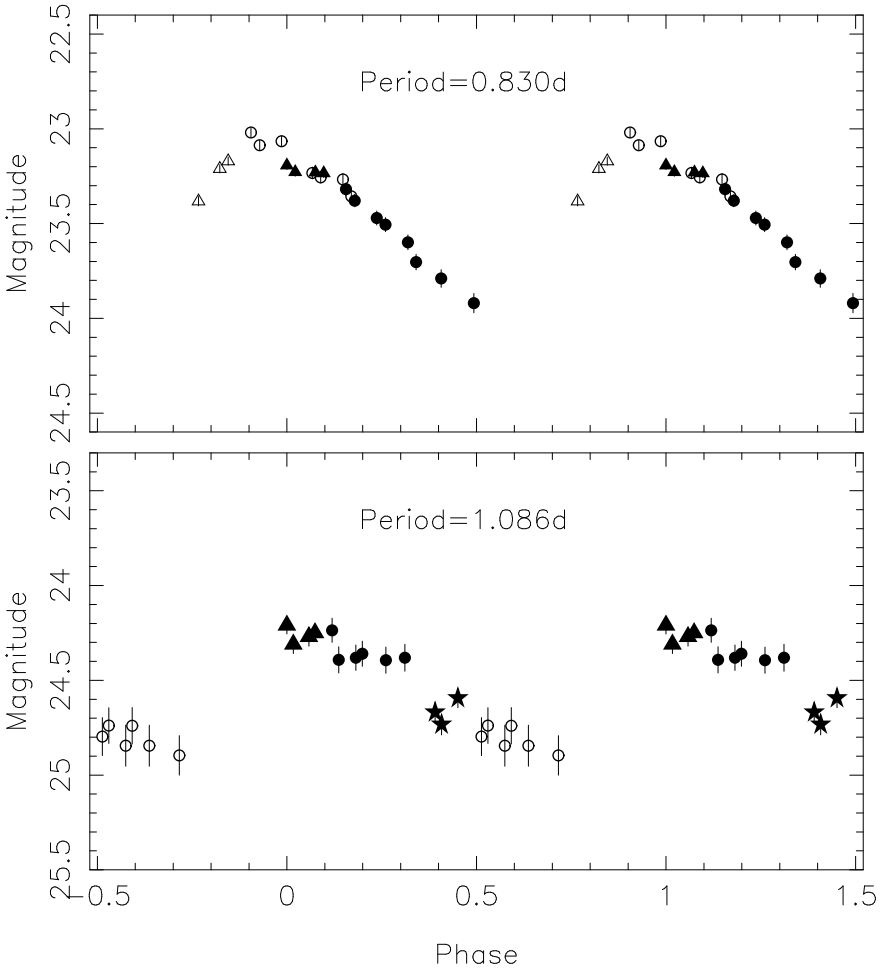

Fig. 6.— Light curves for 1 definite (WF2-1398; upper panel) and 1 probable (WF2-1710; lower panel) Anomalous Cepheid variables in And III. Two cycles are plotted for each star, with the filled and unfilled symbols representing the two sets of observations. F450W magnitudes are shown as circles while F555W magnitudes are shown as triangles. For WF2-1398, a constant F450W–F555W color of 0.20 mag has been assumed to place the F555W observations with those for F450W. For WF2-1710 the color values used were 0.15 and 0.40 mag, respectively. The error bars are those from photon statistics and the period adopted for each star is given in the panels.

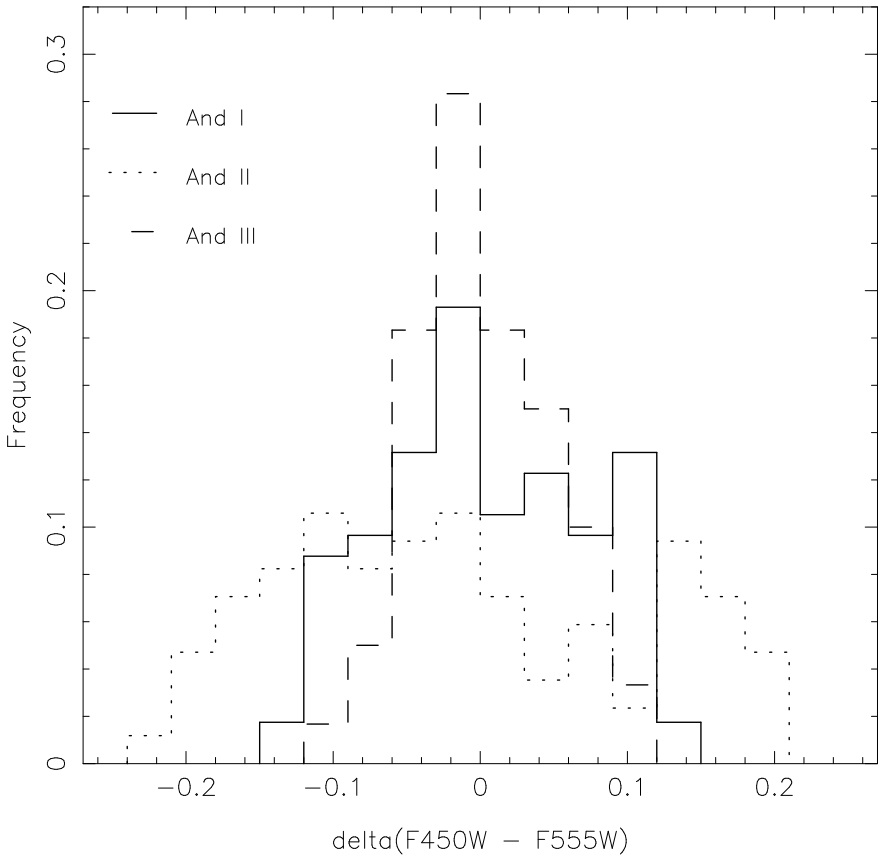

Fig. 7.— Normalized histograms of observed F450W–F555W residuals from the mean giant branches for And I (solid line), And II (dotted line) and And III (dashed line). The sample sizes are 114, 85 and 60 stars, respectively. For all three dSphs, the photometric errors for the F450W–F555W colors are 0.03 mag, the bin size, or less.

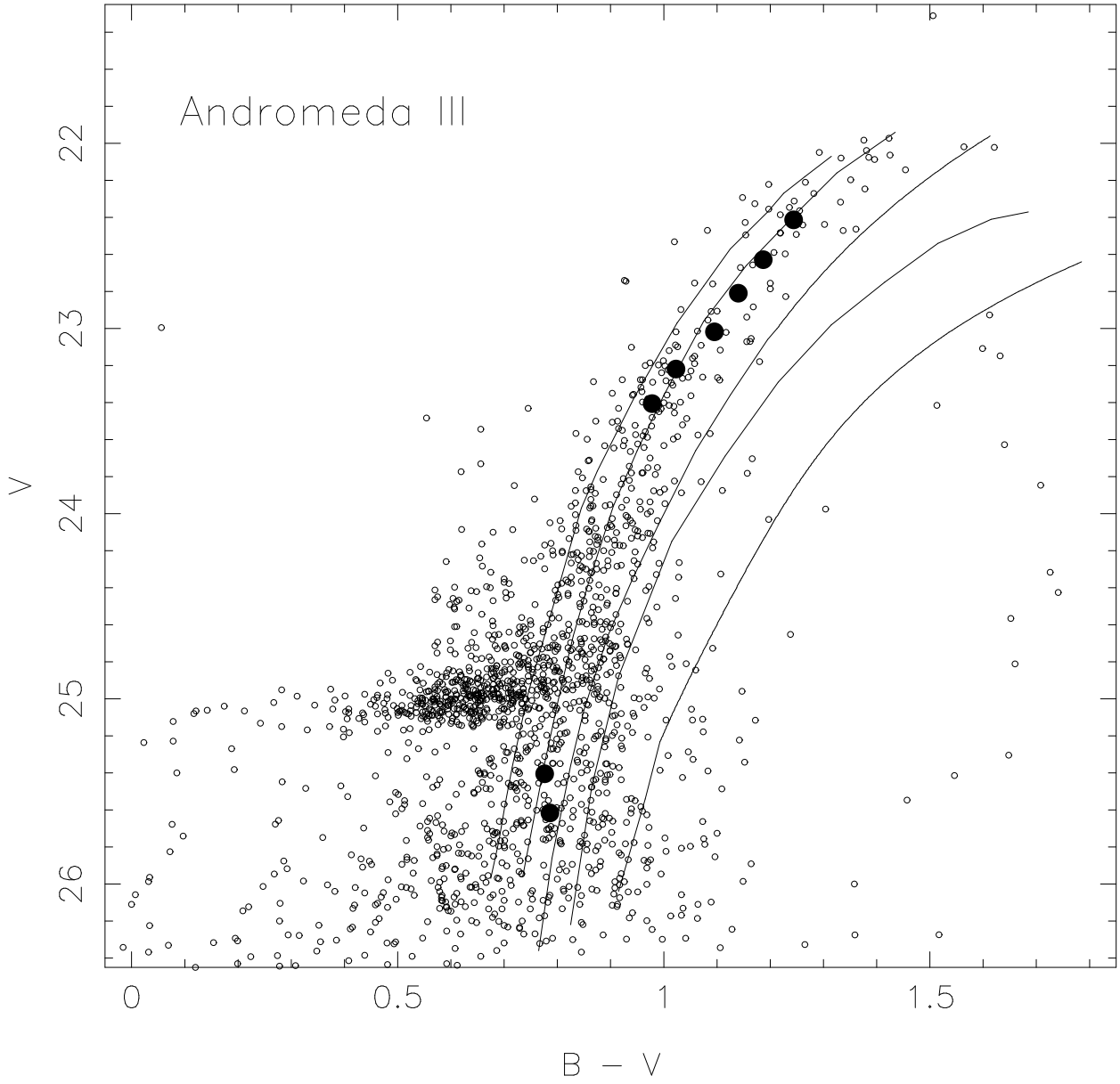

Fig. 8.— The color-magnitude diagram from Fig. 3, excluding the candidate variable stars, is shown superposed with red giant branches from the standard globular clusters M68 ([Fe/H] = –2.09), M55 ([Fe/H] = –1.82), NGC 6752 ([Fe/H] = –1.54), NGC 362 ([Fe/H] = –1.28), and 47 Tuc ([Fe/H] = –0.71). The globular cluster data have been placed in this diagram using $(m - M)_V = 24.56$ and $E(B - V) = 0.055$ for And III. The filled symbols give the mean giant branch colors for bins of ± 0.1 mag in V.

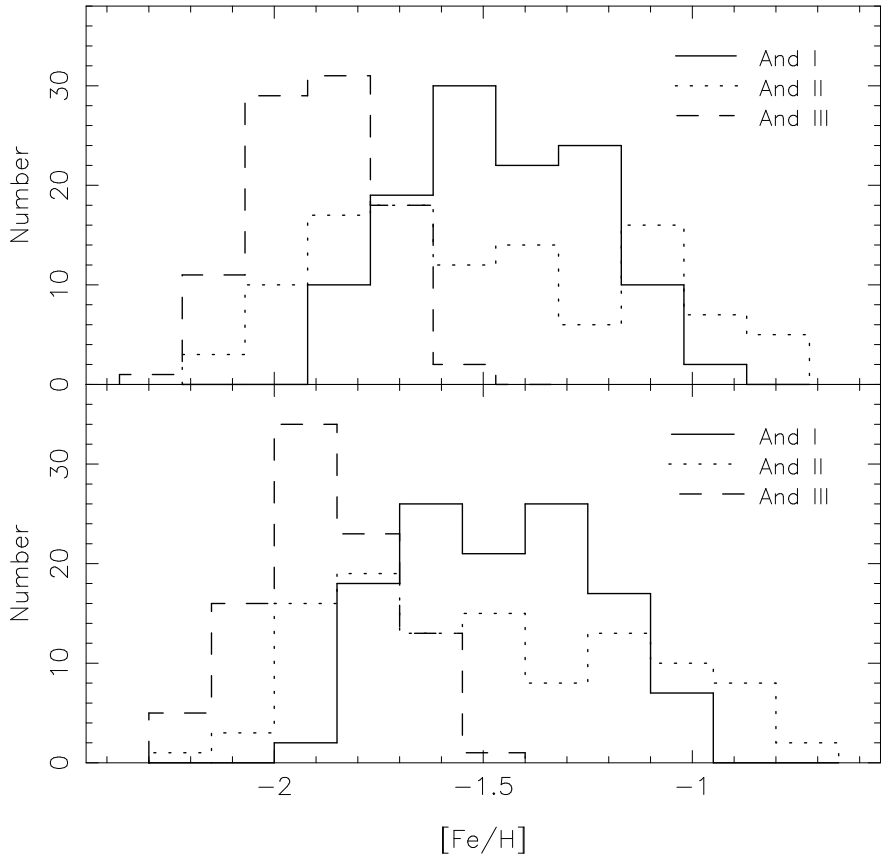

Fig. 9.— Histograms of observed abundance distributions derived from red giant branch colors for And I (solid line), And II (dotted line), both from Paper II, and And III (dashed line). The sample sizes are 117, 108 and 92 stars, respectively, and the average error in the individual [Fe/H] values is 0.10 dex, or less. The bin size is 0.15 dex and the two panels show the effect of moving the centers of the histogram bins by 0.07 dex.

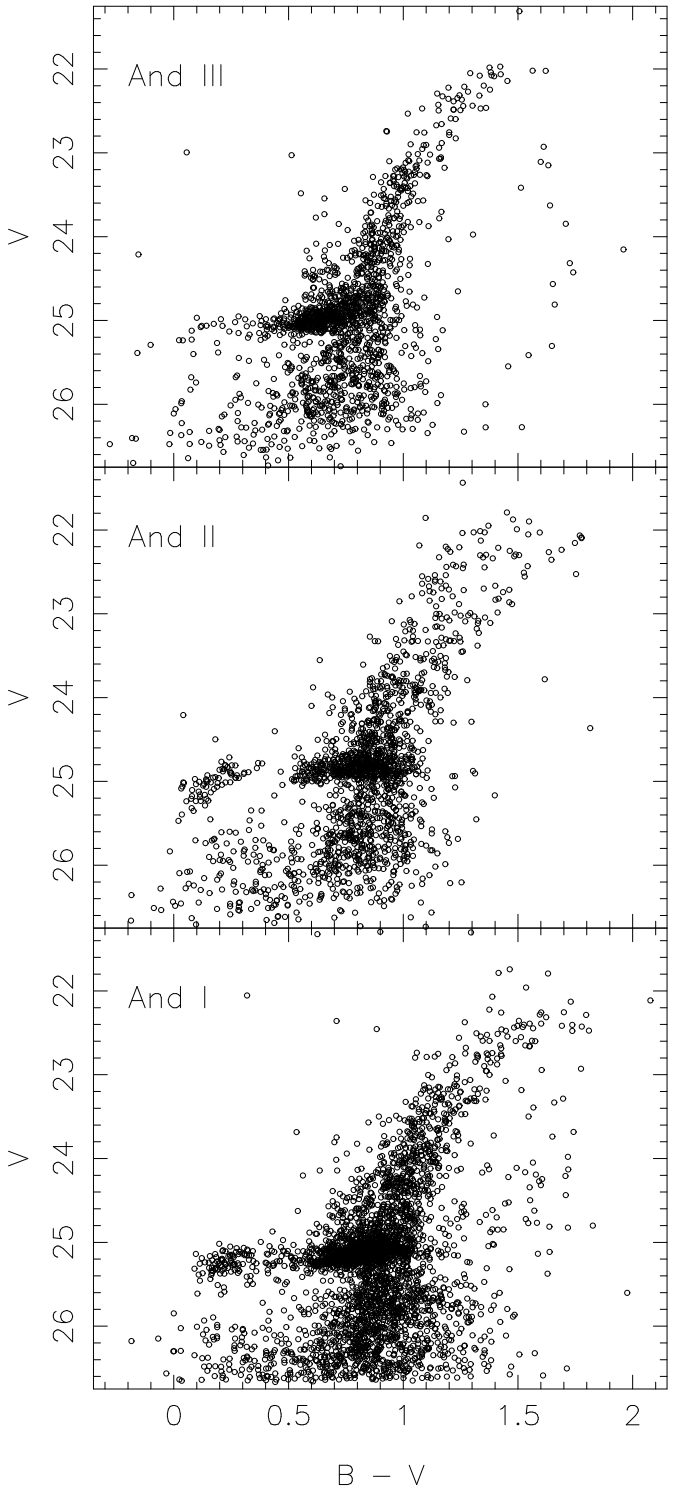

Fig. 10.— Color-magnitude diagrams for And III (upper), And II (middle) and And I (lower) from our WFPC2 programs.

Table 1. Photometric Errors.

F555W	Mean Error in F555W	Mean Error in F450W–F555W	F450W	Mean Error in F450W
21.5–23.0	0.013	0.018	22.0–24.4	0.022
23.0–24.0	0.016	0.026	24.4–24.9	0.030
24.0–24.5	0.024	0.040	24.9–25.4	0.044
24.5–25.0	0.035	0.058	25.4–25.8	0.054
25.0–25.4	0.043	0.068	25.8–26.2	0.078
25.4–25.8	0.060	0.099	26.2–26.6	0.111
25.8–26.1	0.078	0.136	26.6–26.9	0.145
26.1–26.4	0.107	0.180	26.9–27.2	0.187